A Constrained Representation Theorem for Well-Shaped Interval Type-2 Fuzzy Sets, and the Corresponding Constrained Uncertainty Measures

Dongrui Wu, *Senior Member, IEEE*, Hai-Tao Zhang, *Senior Member, IEEE*, and Jian Huang, *Senior Member, IEEE*

***Abstract*—The representation theorem for interval type-2 fuzzy sets (IT2 FSs), proposed by Mendel and John, states that an IT2 FS is a combination of all its embedded type-1 (T1) FSs, which can be nonconvex and/or subnormal. These nonconvex and/or subnormal embedded T1 FSs are included in developing many theoretical results for IT2 FSs, including uncertainty measures, the linguistic weighted averages (LWAs), the ordered LWAs (OLWAs), the linguistic weighted power means (LWPMs), etc. However, convex and normal T1 FSs are used in most fuzzy logic applications, particularly computing with words. In this paper, we propose a constrained representation theorem (CRT) for well-shaped IT2 FSs using only its convex and normal embedded T1 FSs, and show that IT2 FSs generated from three word encoding approaches and four computing with words engines (LWAs, OLWAs, LWPMs, and perceptual reasoning) are all well-shaped IT2 FSs. We also compute five constrained uncertainty measures (centroid, cardinality, fuzziness, variance, and skewness) for well-shaped IT2 FSs using the CRT. The CRT and the associated constrained uncertainty measures can be useful in computing with words, IT2 fuzzy logic system design using the principles of uncertainty, and measuring the similarity between two well-shaped IT2 FSs.**

***Index Terms*—Convex fuzzy sets, interval type-2 fuzzy sets (IT2 FSs), normal fuzzy sets, representation theorem (RT), uncertainty measures.**

I. Introduction

TYPE-2 fuzzy sets (T2 FSs) and systems [21], [48] have attracted wide-spread research interest in the last 15 years and have been successfully applied to many problems [5], [7], [8], [24], [31], [46], as evidenced in Fig. 1, which shows the number of publications per year, when searched in Google Scholar using the exact phrase "type 2 fuzzy" excluding citations and patents.[1] Observe that the trend is almost exponential.

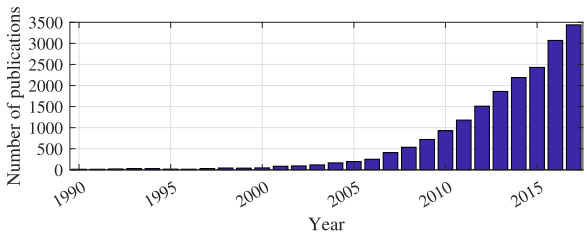

Fig. 1. Number of Google Scholar items on type-2 fuzzy logic.

Interval type-2 (IT2) FSs are to date the most widely used kind of T2 FSs. An IT2 FS $\tilde{A}$ is described as [21]

$$\tilde{A} = \int_{x\in X}\int_{u\in J_x} 1/(x,u) = \int_{x\in X}\left[\int_{u\in J_x} 1/u\right]\Big/ x \quad (1)$$

where x is the *primary variable*, J_x, an interval in $[0,1]$, is the *primary membership* of x, u is the *secondary variable*, and $\int_{u\in J_x} 1/u$ is the *secondary membership function* (MF) at x. Uncertainty about $\tilde{A}$ is conveyed by the union of all of the primary memberships, called the *footprint of uncertainty* of $\tilde{A}$ [FOU($\tilde{A}$)], i.e.,

$$\text{FOU}(\tilde{A}) = \bigcup_{x\in X} J_x. \quad (2)$$

An IT2 FS is shown in Fig. 2. The FOU is shown as the shaded region. It is bounded by an *upper MF* (UMF) $\bar{A}$ and a *lower MF* (LMF) $\underline{A}$, both of which are T1 FSs; consequently, the membership of each element of an IT2 FS is an interval $[u_{\underline{A}}(x), u_{\bar{A}}(x)]$.

Trapezoidal IT2 FSs, whose UMF and LMF are both trapezoidal (triangular MFs are special cases of trapezoidal MFs), are frequently used in practice, especially in computing with words [24]. Nine numbers, shown as $[a,b,c,d,e,f,g,l,h]$ in Fig. 2, can be conveniently used to represent such an IT2 FS.

Manuscript received December 8, 2017; revised July 2, 2018; accepted September 28, 2018. Date of publication October 4, 2018; date of current version June 3, 2019. This work was supported by the National Natural Science Foundation of China under Grant 61873321. *(Corresponding authors: Hai-Tao Zhang and Jian Huang.)*

D. Wu is with the Key Laboratory of the Ministry of Education for Image Processing and Intelligent Control, School of Automation, Huazhong University of Science and Technology, Wuhan 430074, China (e-mail: drwu09@gmail.com).

H.-T. Zhang is with the Key Laboratory of the Ministry of Education for Image Processing and Intelligent Control, School of Automation, Huazhong University of Science and Technology, Wuhan 430074, China, and also with the State Key Lab of Digital Manufacturing Equipment and Technology, Huazhong University of Science and Technology, Wuhan 430074, China (e-mail: zht@mail.hust.edu.cn).

J. Huang is with the Key Laboratory of the Ministry of Education for Image Processing and Intelligent Control, School of Automation, Huazhong University of Science and Technology, Wuhan 430074, China, and also with the Beijing Advanced Innovation Center of Intelligent Robots and Systems, Beijing 100081, China (e-mail: huang_jan@mail.hust.edu.cn).

Color versions of one or more of the fi ures in this paper are available online at http://ieeexplore.ieee.org.

Digital Object Identifier 10.1109/TFUZZ.2018.2874018

[1] We did not count the number of publications about interval-valued fuzzy sets and systems here. The numbers would be larger if we did that.

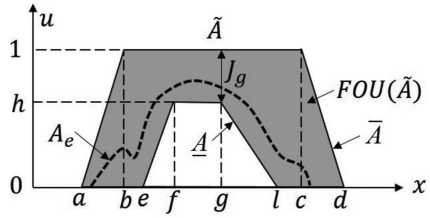

Fig. 2. Trapezoidal IT2 FS $\tilde{A}$. A_e is an embedded T1 FS, which can be nonconvex and/or subnormal.

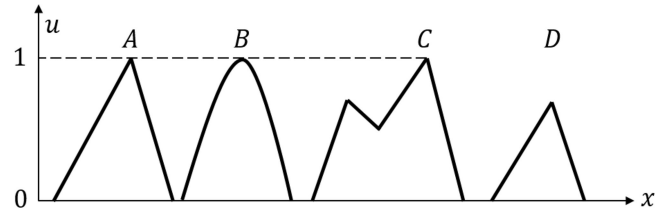

Fig. 3. Four T1 FSs, where A and B are convex and normal, C is nonconvex and normal, and D is convex and subnormal.

Among them, $[a, b, c, d]$ determines the UMF, and $[e, f, g, l, h]$ determines the LMF, where h is the height of the LMF.

Note that an IT2 FS can also be represented as

$$\tilde{A} = 1/\text{FOU}(\tilde{A}) \tag{3}$$

with the understanding that this means putting a secondary membership of 1 at all points of $\text{FOU}(\tilde{A})$.

For a continuous universe of discourse X, an *embedded T1 FS* A_e is represented as

$$A_e = \int_{x \in X} u(x)/x. \tag{4}$$

An example of A_e is shown in Fig. 2. Observe that it is not necessarily convex and normal.

Mendel and John [22] have presented a representation theorem (RT) for general T2 FSs, which when specialized to IT2 FSs can be expressed as follows.

Mendel–John RT for IT2 FSs: The FOU of an IT2 FS $\tilde{A}$ is the union of all its embedded T1 FSs, i.e.,

$$\text{FOU}(\tilde{A}) = \bigcup A_e. \tag{5}$$

■

The embedded T1 FSs in the Mendel–John RT could be nonconvex and/or subnormal. This RT implies that all these embedded T1 FSs should be considered in deriving theoretical results for IT2 FSs, e.g., uncertainty measures [38], [41], similarity measures [26], [27], [43], subsethood measures [26], [43], linguistic weighted averages (LWA) [24], [36], [39], ordered LWAs (OLWA) [35], [44], linguistic weighted power means (LWPM) [28], and so on. However, in practice, most applications of T1 FLSs use only convex and normal T1 FSs. Additionally, the interval approach (IA) [19], enhanced IA (EIA) [45], and Hao-Mendel approach (HMA) [9], which are three popular methods to construct IT2 FS models for words from surveyed end-point data, are also based on convex and normal T1 FSs, and can only generate convex and normal IT2 FSs. So, a constrained RT (CRT), which considers only convex and normal embedded T1 FSs for an IT2 FS, may be more intuitive. This is our main motivation.

More specifically, this paper makes the following contributions.

1) We propose a CRT for well-shaped IT2 FSs, i.e., the FOU of a well-shaped IT2 FS can be completely covered by its convex and normal embedded T1 FSs.
2) We show that IT2 FSs generated from the IA, EIA, and HMA are well-shaped IT2 FSs, and hence the CRT can be applied to them.
3) We show that IT2 FSs output by the LWAs, OLWAs, LWPMs, or perceptual reasoning (PR) [23], [42] are also well-shaped IT2 FSs, and hence the CRT can be applied to them.
4) We develop algorithms for computing five constrained uncertainty measures (centroid, cardinality, fuzziness, variance, and skewness) for well-shaped IT2 FSs.

Although we focus on trapezoidal IT2 FSs in this paper, our results can also be extended to Gaussian and other IT2 FSs, as long as they are well shaped.

The rest of this paper is organized as follows: Section II introduces the proposed CRT and explains where well-shaped IT2 FSs come from. Section III describes how five constrained uncertainty measures (centroid, cardinality, fuzziness, variance, and skewness) can be computed for well-shaped IT2 FSs based on the CRT. Section IV discusses the advantages and limitations of the CRT. Finally, Section V draws conclusions.

II. CRT for Well-Shaped IT2 FSs Based on Convex and Normal Embedded T1 FSs

In this section, we propose a CRT for well-shaped IT2 FSs based on only convex and normal embedded T1 FSs. Well-shaped IT2 FSs are the main kind of IT2 FSs used in many applications of IT2 FLSs, particularly computing with words [24].

A. Definitions

The definitions of convex and normal T1 FSs and well-shaped IT2 FSs are given first.

Definition 1: [14] A T1 FS A is *convex* if and only if $u_A(\lambda x_1 + (1-\lambda)x_2) \geq \min(u_A(x_1), u_A(x_2))$ for $\forall\, x_1, x_1 \in X$ and $\lambda \in [0, 1]$. ■

Fig. 3 shows three convex T1 FSs A, B, and D, and a nonconvex T1 FS C.

Definition 2: [24] A T1 FS A is *normal* if and only if $\sup_{x \in X} u_A(x) = 1$. ■

Fig. 3 shows three normal T1 FSs A, B, and C, and a subnormal T1 FS D.

Definition 3: An IT2 FS $\tilde{A}$ is *convex and normal* if and only if: 1) its UMF is convex and normal; and 2) its LMF is convex. ■

The IT2 FS $\tilde{A}$ in Fig. 2 is convex and normal.

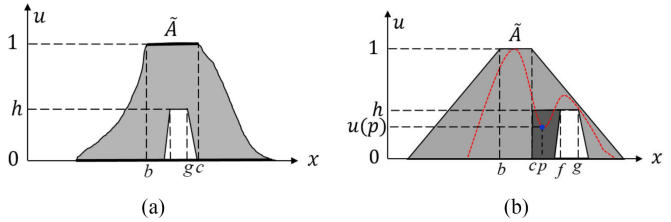

Fig. 4. (a) Well-shaped IT2 FS, which is not necessarily trapezoidal. (b) Trapezoidal IT2 FS, which is convex and normal, but not well shaped.

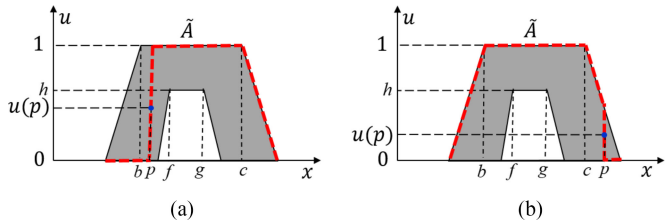

Fig. 5. Illustration of convex and normal embedded T1 FSs which pass through $(p, u(p))$. (a) $p < c$. (b) $p \geq c$.

Let $[b, c]$ be the top base of $\bar{A}$, and $[f, g]$ be the top base of $\underline{A}$, as shown in Fig. 2. Then,

Definition 4: An IT2 FS $\tilde{A}$ is well shaped if and only if: 1) it is convex and normal; and 2) $f \geq b$ and $g \leq c$, i.e., the top base of the LMF is completely within the top base of the UMF. ■

$\tilde{A}$ in Figs. 2 and 4(a) are well shaped. Observe from Fig. 4(a) that $\tilde{A}$ does not need to be trapezoidal to be well shaped. $\tilde{A}$ in Fig. 4(b) is not well shaped, although it is convex and normal, because $g > c$.

B. CRT for Well-Shaped IT2 FSs

In this subsection, we propose a CRT for well-shaped IT2 FSs.

Theorem 1: (*CRT for well-shaped IT2 FSs*) The FOU of a well-shaped IT2 FS is the union of all its convex and normal embedded T1 FSs.

■

For this CRT to be correct, we need to verify that the union of all convex and normal embedded T1 FSs can cover the entire FOU of a well-shaped IT2 FS, as indicated by the following.

Lemma 1: The FOU of a well-shaped IT2 FS can be completely covered by its convex and normal embedded T1 FSs.

■

Proof: Consider an arbitrary point $(p, u(p))$ within the FOU of a well-shaped IT2 FS, whose UMF has top base $[b, c]$. There can be only two cases.

1) $p < c$: We can construct an embedded T1 FS A_e as shown in Fig. 5(a), which starts from the LMF and then switches to the UMF at $x = p$.
2) $p \geq c$: We can construct an embedded T1 FS A_e as shown in Fig. 5(b), which starts from the UMF and then switches to the LMF at $x = p$.

In summary, for an arbitrary point within the FOU of a well-shaped IT2 FS, we can find at least one convex and normal embedded T1 FS which passes through it. So, the FOU of a well-shaped IT2 FS can be completely covered by only its convex and normal embedded T1 FSs. ■

The requirement "$f \geq b$ and $g \leq c$" in Definition 4 of a well-shaped IT2 FS is very important, because of the following.[2]

Lemma 2: The FOU of a convex and normal IT2 FS cannot be completely covered by only its convex and normal embedded T1 FSs, if $f < b$ and/or $g > c$. ■

Proof: We use an example to demonstrate the case for $f < b$. The case for $g > c$ can be shown similarly.

Consider the point $(p, u(p))$ in Fig. 4(b), which belongs to a convex and normal, but not well-shaped, IT2 FS. For any normal embedded T1 FS to pass through $(p, u(p))$, it must have membership 1 at at least one point on the left of $x = p$ (because no point on the right of $x = p$ can have membership 1), i.e., at least one point on the left of $x = p$ must have membership larger than $u(p)$. Because $u(p)$ is smaller than h (the height of the LMF), any embedded T1 FS passing through $(p, u(p))$ must also have some memberships larger than $u(p)$ on the right of $x = p$. In summary, for every normal embedded T1 FS, there are points on both sides of $x = p$ whose memberships are larger than $u(p)$. So, every normal embedded T1 FS passing through $(p, u(p))$ is nonconvex. In other words, $(p, u(p))$ cannot be covered by any embedded T1 FS that is both convex and normal. In fact, no point within the dark trapezoidal area in Fig. 4(b) can be covered by any convex and normal embedded T1 FS. ■

C. Where Well-Shaped IT2 FSs Come From

In this subsection, we will show that IT2 FSs constructed from three different word encoding approaches (IA [19], EIA [45], and HMA [9]) are well-shaped IT2 FSs, and IT2 FSs output by the perceptual computer [24], with four different computing with words engines (LWA [36], [39], OLWA [35], [44], LWPM [28], and PR [23], [42]), are also well-shaped IT2 FSs.

Theorem 2: All IT2 FSs constructed from the IA are well shaped. ■

Proof: The IA [19] consists of two parts, the *Data Part* and the *FS Part*. In the *Data Part*, the interval end-point data for each word are first obtained from survey, and then they go through bad data processing, outlier processing, tolerance limit processing, and reasonable interval processing. In each step, some intervals may be removed. In the *FS Part*, the nature of the FOU (interior, left shoulder, or right shoulder, see Fig. 6) is first determined, and then each of the word's data intervals is individually mapped into its respective T1 interior, left-shoulder or right-shoulder MF (see Fig. 7), after which the LMF and UMF of the IT2 FS are computed. This proof only concerns the last step, i.e., how the LMF and UMF of the IT2 FSs in Fig. 6 are computed from the T1 MFs in Fig. 7.

Consider first the case that the resulting IT2 FS is a left shoulder, as shown in Fig. 6(a). Its parameters are computed as [19]

$$\underline{a}_{\mathrm{MF}} = \min_{i=1,\ldots,m^*} \left\{ a_{\mathrm{MF}}^{(i)} \right\} \tag{6}$$

[2]Note that this requirement was not considered in [33]. As a result, the CRT in [33] has a flaw, which is corrected in this paper.

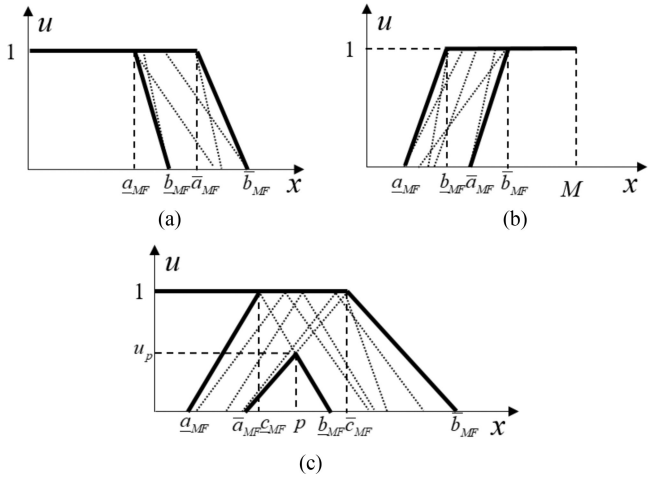

Fig. 6. Examples of the union of (dashed) T1 MFs. The thick lines are the LMFs and UMFs for the FOU. (a) Left-shoulder, (b) right-shoulder, and (c) interior FOU.

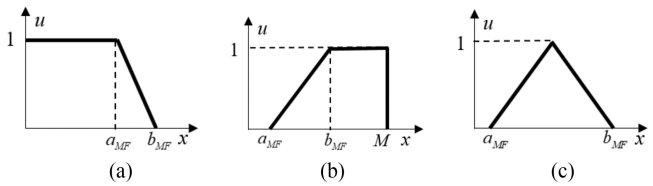

Fig. 7. Examples of the T1 MFs mapped from interval end-points data. (a) Left-shoulder, (b) right-shoulder, and (c) interior MF.

$$\bar{a}_{\mathrm{MF}} = \max_{i=1,\ldots,m^*} \left\{ a_{\mathrm{MF}}^{(i)} \right\} \tag{7}$$

$$\underline{b}_{\mathrm{MF}} = \min_{i=1,\ldots,m^*} \left\{ b_{\mathrm{MF}}^{(i)} \right\} \tag{8}$$

$$\bar{b}_{\mathrm{MF}} = \max_{i=1,\ldots,m^*} \left\{ b_{\mathrm{MF}}^{(i)} \right\} \tag{9}$$

where $a_{\mathrm{MF}}^{(i)}$ and $b_{\mathrm{MF}}^{(i)}$ stand for a_{MF} and b_{MF} in Fig. 7(a) for the ith T1 MF in the *FS Part*, and m^* is the total number of T1 MFs in the *FS Part*. Because all m^* such T1 MFs are normal, the resulting left-shoulder IT2 FS is also normal. Since $a_{\mathrm{MF}}^{(i)} \leq b_{\mathrm{MF}}^{(i)}$ $\forall i = 1, \ldots, m^*$, it follows from (6) and (8) that $\underline{a}_{\mathrm{MF}} \leq \underline{b}_{\mathrm{MF}}$, and from (7) and (9) that $\bar{a}_{\mathrm{MF}} \leq \bar{b}_{\mathrm{MF}}$, i.e., the resulting IT2 FS is convex. Together these mean the resulting left-shoulder IT2 FS is convex and normal. Since the top base of the UMF is $[0, \bar{a}_{\mathrm{MF}}]$ and the top base of the LMF is $[0, \underline{a}_{\mathrm{MF}}]$, whereas $\underline{a}_{\mathrm{MF}} \leq \bar{a}_{\mathrm{MF}}$, the top base of the LMF is within the top base of the UMF. In summary, the resulting left-shoulder IT2 FS is well shaped.

The proof for the right shoulder in Fig. 6(b) is very similar, so it is omitted here.

Next we consider the case that the resulting IT2 FS is an interior FOU, as shown in Fig. 6(c). In addition to $\underline{a}_{\mathrm{MF}}$, $\bar{a}_{\mathrm{MF}}$, $\underline{b}_{\mathrm{MF}}$, and $\bar{b}_{\mathrm{MF}}$ in (6)–(9), its parameters $\underline{c}_{\mathrm{MF}}$, $\bar{c}_{\mathrm{MF}}$, p, and $u(p)$ are computed from the interior T1 MF in Fig. 7(c) as [19]

$$\underline{c}_{\mathrm{MF}} = \min_{i=1,\ldots,m^*} \left\{ c_{\mathrm{MF}}^{(i)} \right\}, \quad \bar{c}_{\mathrm{MF}} = \max_{i=1,\ldots,m^*} \left\{ c_{\mathrm{MF}}^{(i)} \right\} \tag{10}$$

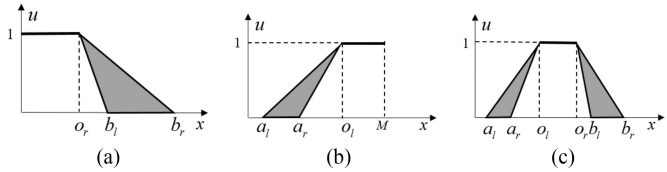

Fig. 8. Examples of the FOUs generated from the HMA. (a) Left-shoulder, (b) right-shoulder, and (c) interior FOU.

$$p = \frac{\underline{b}_{\mathrm{MF}}(\bar{c}_{\mathrm{MF}} - \bar{a}_{\mathrm{MF}}) + \bar{a}_{\mathrm{MF}}(\underline{b}_{\mathrm{MF}} - \underline{c}_{\mathrm{MF}})}{(\bar{c}_{\mathrm{MF}} - \bar{a}_{\mathrm{MF}}) + (\underline{b}_{\mathrm{MF}} - \underline{c}_{\mathrm{MF}})} \tag{11}$$

$$u(p) = \frac{\underline{b}_{\mathrm{MF}} - p}{\underline{b}_{\mathrm{MF}} - \underline{c}_{\mathrm{MF}}} \tag{12}$$

where

$$c_{\mathrm{MF}}^{(i)} = \frac{a_{\mathrm{MF}}^{(i)} + b_{\mathrm{MF}}^{(i)}}{2}. \tag{13}$$

Because all m^* T1 MFs are normal, the resulting interior IT2 FS is normal. Because $a_{\mathrm{MF}}^{(i)} \leq c_{\mathrm{MF}}^{(i)} \leq b_{\mathrm{MF}}^{(i)}$, $\forall i = 1, \ldots, m^*$, it follows that $\bar{a}_{\mathrm{MF}} \leq p \leq \underline{b}_{\mathrm{MF}}$ and $\underline{a}_{\mathrm{MF}} \leq \underline{c}_{\mathrm{MF}} \leq \bar{c}_{\mathrm{MF}} \leq \bar{b}_{\mathrm{MF}}$, i.e., the resulting interior IT2 FS is also convex. Together these mean that the resulting interior IT2 FS is convex and normal. The LMF from the IA is always a triangle with apex $(p, u(p))$. From Fig. 6(c), we can observe that this apex is the intersection of the line connecting $\underline{c}_{\mathrm{MF}}$ and $\underline{b}_{\mathrm{MF}}$ with the line connecting $\bar{c}_{\mathrm{MF}}$ and $\bar{a}_{\mathrm{MF}}$, so $\underline{c}_{\mathrm{MF}} \leq p \leq \bar{c}_{\mathrm{MF}}$, i.e., the apex of the LMF is within the top base of the UMF. Consequently, the resulting interior IT2 FS is well shaped. ■

Theorem 3: All IT2 FSs constructed from the EIA are well shaped. ■

This proof is very similar to the proof for Theorem 2, so it is left to the reader.

Theorem 4: All IT2 FSs constructed from the HMA are well shaped. ■

Proof: The HMA [9] can construct an FOU from a group of subjects and also a single subject. We only give the proof for the first case here, as the proof for the second is very similar.

The HMA for a group of subjects also has two parts: the data part and the FS part. Its data part is the same as that in the EIA and similar to that in the IA, i.e., it uses bad data/outlier removal, tolerance-limit processing, and reasonable interval processing to clean up the intervals obtained from survey. The FS part computes the overlap $[o_l, o_r]$ of the remaining intervals, and $[o_l, o_r]$ then becomes the common top base of both the UMF and the LMF, as shown in Fig. 8. The FS part also computes a_l, a_r, b_l, and b_r next from the remaining intervals (the details are not important to this proof), and makes sure $a_l \leq a_r \leq o_l \leq o_r \leq b_l \leq b_r$. It then connects the four points $(a_l, 0)$, $(o_l, 1)$, $(o_r, 1)$, and $(b_r, 0)$ to form a trapezoidal normal UMF, and the four points $(a_r, 0)$, $(o_l, 1)$, $(o_r, 1)$, and $(b_l, 0)$ to form a trapezoidal normal LMF, as shown in Fig. 8 ($a_l = a_r = o_l = 0$ for the left shoulder, and $b_l = b_r = o_r = M$ for the right shoulder). Clearly, both the UMF and the LMF are convex and normal, and hence the IT2 FS is convex and normal. Additionally, the top base of the LMF is always the same as the top base of the UMF, and hence the IT2 FS is well shaped. ■

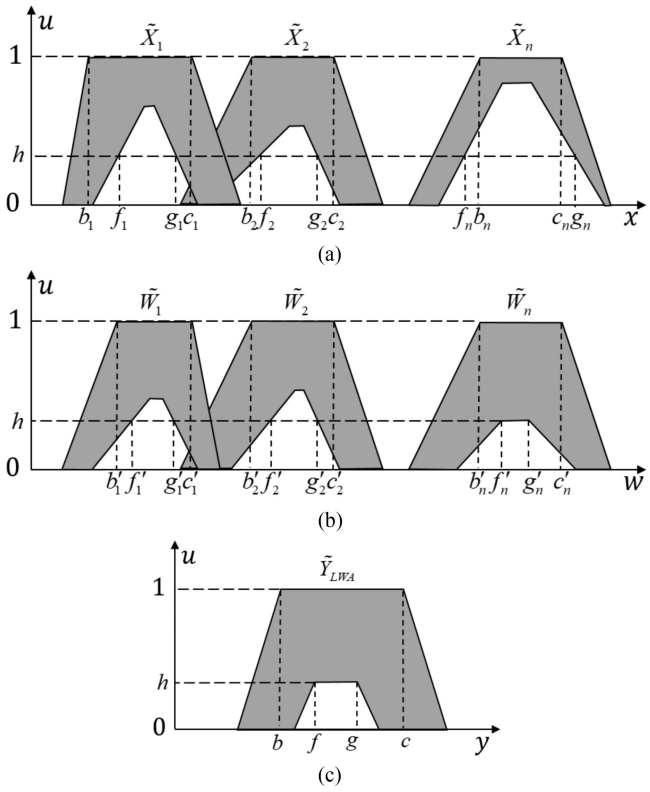

Fig. 9. LWA. (a) $\tilde{X}_i$. (b) $\tilde{W}_i$. (c) $\tilde{Y}_{\text{LWA}}$.

Theorem 5: If all input IT2 FSs are well shaped, then the IT2 FS computed from the LWA is also well shaped. ■

Proof: Let $\tilde{X}_i$, $\tilde{W}_i$, and $\tilde{Y}$ be IT2 FSs shown in Fig. 9. An LWA [36], [39] is defined as

$$\tilde{Y}_{\text{LWA}} = \frac{\sum_{i=1}^{n} \tilde{W}_i \tilde{X}_i}{\sum_{i=1}^{n} \tilde{W}_i}. \tag{14}$$

It has been shown [36], [39] that the UMF $\bar{Y}_{\text{LWA}}$ and the LMF $\underline{Y}_{\text{LWA}}$ can be computed by fuzzy weighted averages

$$\bar{Y}_{\text{LWA}} = \frac{\sum_{i=1}^{n} \bar{W}_i \bar{X}_i}{\sum_{i=1}^{n} \bar{W}_i} \tag{15}$$

$$\underline{Y}_{\text{LWA}} = \frac{\sum_{i=1}^{n} \underline{W}_i \underline{X}_i}{\sum_{i=1}^{n} \underline{W}_i}. \tag{16}$$

The height of $\underline{Y}_{\text{LWA}}$ is h, which is the minimum height of all $\underline{X}_i$ and $\underline{W}_i$.

$\bar{Y}_{\text{LWA}}$ and $\underline{Y}_{\text{LWA}}$ are computed using α-cut decomposition [18]. When all $\bar{X}_i$ and $\bar{W}_i$ are well-shaped IT2 FSs, all $\bar{X}_i$ and $\bar{W}_i$ are normal; consequently, $\bar{Y}_{\text{LWA}}$ is also normal. Next we need to show $\bar{Y}_{\text{LWA}}$ is also convex.

Consider two α-cuts α_1 and α_2, where $\alpha_1 < \alpha_2$. Let the α_j α-cut on $\bar{X}_i$ be $[x_{ij,l}, x_{ij,r}]$, on $\bar{W}_i$ be $[w_{ij,l}, w_{ij,r}]$, and the corresponding α-cut on $\bar{Y}_{\text{LWA}}$ be $[y_{j,l}, y_{j,r}]$, $i = 1, \ldots, n$, $j = 1, 2$. Then, $x_{i1,l} \le x_{i2,l}$, $x_{i1,r} \ge x_{i2,r}$, $w_{i1,l} \le w_{i2,l}$, and $w_{i1,r} \ge w_{i2,r}$. $y_{j,l}$ and $y_{j,r}$ are computed as [36], [39]

$$y_{j,l} = \min_{w_i \in [w_{ij,l}, w_{ij,r}]} \frac{\sum_{i=1}^{n} w_i x_{ij,l}}{\sum_{i=1}^{n} w_i},\ j = 1, 2 \tag{17}$$

$$y_{j,r} = \max_{w_i \in [w_{ij,l}, w_{ij,r}]} \frac{\sum_{i=1}^{n} w_i x_{ij,r}}{\sum_{i=1}^{n} w_i},\ j = 1, 2. \tag{18}$$

To show $\bar{Y}_{\text{LWA}}$ is convex, we only need to show that $y_{j,l}$ is nondecreasing with the increase of α_j, and $y_{j,r}$ is nonincreasing with the increase of α_j, i.e., $y_{2,l} \ge y_{1,l}$ and $y_{2,r} \le y_{1,r}$ when $\alpha_1 < \alpha_2$

$$\begin{aligned} y_{2,l} &= \min_{w_i \in [w_{i2,l}, w_{i2,r}]} \frac{\sum_{i=1}^{n} w_i x_{i2,l}}{\sum_{i=1}^{n} w_i} \\ &\ge \min_{w_i \in [w_{i2,l}, w_{i2,r}]} \frac{\sum_{i=1}^{n} w_i x_{i1,l}}{\sum_{i=1}^{n} w_i} \\ &\ge \min_{w_i \in [w_{i1,l}, w_{i1,r}]} \frac{\sum_{i=1}^{n} w_i x_{i1,l}}{\sum_{i=1}^{n} w_i} = y_{1,l} \end{aligned} \tag{19}$$

$$\begin{aligned} y_{2,r} &= \max_{w_i \in [w_{i2,l}, w_{i2,r}]} \frac{\sum_{i=1}^{n} w_i x_{i2,r}}{\sum_{i=1}^{n} w_i} \\ &\le \max_{w_i \in [w_{i2,l}, w_{i2,r}]} \frac{\sum_{i=1}^{n} w_i x_{i1,r}}{\sum_{i=1}^{n} w_i} \\ &\le \max_{w_i \in [w_{i1,l}, w_{i1,r}]} \frac{\sum_{i=1}^{n} w_i x_{i1,r}}{\sum_{i=1}^{n} w_i} = y_{1,r}. \end{aligned} \tag{20}$$

So, $\bar{Y}_{\text{LWA}}$ is convex. In a similar way, we can also show that $\underline{Y}_{\text{LWA}}$ is convex. Consequently, $\tilde{Y}_{\text{LWA}}$ is convex and normal.

Let the top base of $\bar{Y}_{\text{LWA}}$ be $[b, c]$, and the top base of $\underline{Y}_{\text{LWA}}$ be $[f, g]$, as shown in Fig. 9(c). Next we need to show $f \ge b$ and $g \le c$. From the LWA algorithm [36], [39], we have

$$b = \min_{w_i \in [b_i', c_i']} \frac{\sum_{i=1}^{n} b_i w_i}{\sum_{i=1}^{n} w_i}, \qquad c = \max_{w_i \in [b_i', c_i']} \frac{\sum_{i=1}^{n} c_i w_i}{\sum_{i=1}^{n} w_i}$$

$$f = \min_{w_i \in [f_i', g_i']} \frac{\sum_{i=1}^{n} f_i w_i}{\sum_{i=1}^{n} w_i}, \qquad g = \max_{w_i \in [f_i', g_i']} \frac{\sum_{i=1}^{n} g_i w_i}{\sum_{i=1}^{n} w_i}.$$

Because $f_i \ge b_i$, and $g_i \le c_i$, it follows that

$$\begin{aligned} f &= \min_{w_i \in [f_i', g_i']} \frac{\sum_{i=1}^{n} f_i w_i}{\sum_{i=1}^{n} w_i} \ge \min_{w_i \in [f_i', g_i']} \frac{\sum_{i=1}^{n} b_i w_i}{\sum_{i=1}^{n} w_i} \\ &\ge \min_{w_i \in [b_i', c_i']} \frac{\sum_{i=1}^{n} b_i w_i}{\sum_{i=1}^{n} w_i} = c \end{aligned} \tag{21}$$

$$\begin{aligned} g &= \max_{w_i \in [f_i', g_i']} \frac{\sum_{i=1}^{n} g_i w_i}{\sum_{i=1}^{n} w_i} \le \max_{w_i \in [f_i', g_i']} \frac{\sum_{i=1}^{n} c_i w_i}{\sum_{i=1}^{n} w_i} \\ &\le \max_{w_i \in [b_i', c_i']} \frac{\sum_{i=1}^{n} c_i w_i}{\sum_{i=1}^{n} w_i} = c. \end{aligned} \tag{22}$$

So, $\tilde{Y}_{\text{LWA}}$ is a well-shaped IT2 FS. ■

Theorem 6: If all input IT2 FSs are well shaped, then the IT2 FS computed from the OLWA is also well shaped. ■

The OLWA is defined as [35], [44]

$$\tilde{Y}_{\text{OLWA}} = \frac{\sum_{i=1}^{n} \tilde{W}_i \tilde{X}_{\sigma(i)}}{\sum_{i=1}^{n} \tilde{W}_i} \tag{23}$$

where $\sigma : \{1, \ldots, n\} \to \{1, \ldots, n\}$ is a permutation function such that $\{\tilde{X}_{\sigma(1)}, \tilde{X}_{\sigma(2)}, \ldots, \tilde{X}_{\sigma(n)}\}$ are in descending order. Clearly, once ordered, the OLWA becomes an LWA, and hence Theorem 6 is true.

Theorem 7: If all input IT2 FSs are well shaped, then the IT2 FS computed from the LWPM is also well shaped. ■

Proof: The LWPM is defined as[3] [28]

$$\tilde{Y}_{\text{LWPM}} = \lim_{q \to q^*} \left(\frac{\sum_{i=1}^n \tilde{W}_i \tilde{X}_i^q}{\sum_{i=1}^n \tilde{W}_i} \right)^{1/q}. \tag{24}$$

Clearly, the LWA is a special case of the LWPM when $q^* = 1$. As in the LWA, the UMF and LMF of $\tilde{Y}_{\text{LWPM}}$ are also computed as[4] [28]

$$\bar{Y}_{\text{LWPM}} = \lim_{q \to q^*} \left(\frac{\sum_{i=1}^n \bar{W}_i \bar{X}_i^q}{\sum_{i=1}^n \bar{W}_i} \right)^{1/q} \tag{25}$$

$$\underline{Y}_{\text{LWPM}} = \lim_{q \to q^*} \left(\frac{\sum_{i=1}^n \underline{W}_i \underline{X}_i^q}{\sum_{i=1}^n \underline{W}_i} \right)^{1/q} \tag{26}$$

from α-cut decomposition.

When $q^* = \infty$, $\tilde{Y}_{\text{LWPM}}$ is independent of $\tilde{W}_i$, and it equals the maximum $\tilde{X}_i$. When $q^* = -\infty$, $\tilde{Y}_{\text{LWPM}}$ is also independent of $\tilde{W}_i$, and it equals the minimum $\tilde{X}_i$. Since all $\tilde{X}_i$ are well-shaped IT2 FSs, $\tilde{Y}_{\text{LWPM}}$ is also a well-shaped IT2 FS when $q^* = \pm\infty$.

Next we consider a finite q^*. Without loss of generality, we focus only on $q^* > 0$. The case for $q^* < 0$ can be shown very similarly.

When all $\bar{X}_i$ and $\bar{W}_i$ are normal, $\bar{Y}_{\text{LWPM}}$ is normal. Next we show that $\bar{Y}_{\text{LWPM}}$ is convex when $q^* > 0$.

Consider two α-cuts α_1 and α_2, where $\alpha_1 < \alpha_2$. Let the α_j α-cut on $\bar{X}_i$ be $[x_{ij,l}, x_{ij,r}]$, on $\bar{W}_i$ be $[w_{ij,l}, w_{ij,r}]$, and the corresponding α-cut on $\bar{Y}_{\text{LWPM}}$ be $[y_{j,l}, y_{j,r}]$, $i = 1, \ldots, n$, $j = 1, 2$. Then, $x_{i1,l} \le x_{i2,l}$, $x_{i1,r} \ge x_{i2,r}$, $w_{i1,l} \le w_{i2,l}$, and $w_{i1,r} \ge w_{i2,r}$. $y_{j,l}$ and $y_{j,r}$ are computed as [28]

$$y_{j,l} = \min_{w_i \in [w_{ij,l}, w_{ij,r}]} \left(\frac{\sum_{i=1}^n w_i x_{ij,l}^{q^*}}{\sum_{i=1}^n w_i} \right)^{1/q^*}, \ j = 1, 2 \tag{27}$$

$$y_{j,r} = \max_{w_i \in [w_{ij,l}, w_{ij,r}]} \left(\frac{\sum_{i=1}^n w_i x_{ij,r}^{q^*}}{\sum_{i=1}^n w_i} \right)^{1/q^*}, \ j = 1, 2. \tag{28}$$

To show that $\bar{Y}_{\text{LWA}}$ is convex, we only need to show that $y_{j,l}$ is nondecreasing with the increase of α_j, and $y_{j,r}$ is nonincreasing with the increase of α_j, i.e., $y_{2,l} \ge y_{1,l}$ and $y_{2,r} \le y_{1,r}$ when $\alpha_1 < \alpha_2$.

Because both z^{q^*} and z^{1/q^*} increase with z when $q^* > 0$, we have

$$y_{2,l} = \min_{w_i \in [w_{i2,l}, w_{i2,r}]} \left(\frac{\sum_{i=1}^n w_i x_{i2,l}^{q^*}}{\sum_{i=1}^n w_i} \right)^{1/q^*}$$

$$\ge \min_{w_i \in [w_{i2,l}, w_{i2,r}]} \left(\frac{\sum_{i=1}^n w_i x_{i1,l}^{q^*}}{\sum_{i=1}^n w_i} \right)^{1/q^*}$$

$$\ge \min_{w_i \in [w_{i1,l}, w_{i1,r}]} \left(\frac{\sum_{i=1}^n w_i x_{i1,l}^{q^*}}{\sum_{i=1}^n w_i} \right)^{1/q^*} = y_{1,l} \tag{29}$$

$$y_{2,r} = \max_{w_i \in [w_{i2,l}, w_{i2,r}]} \left(\frac{\sum_{i=1}^n w_i x_{i2,r}^{q^*}}{\sum_{i=1}^n w_i} \right)^{1/q^*}$$

$$\le \max_{w_i \in [w_{i2,l}, w_{i2,r}]} \left(\frac{\sum_{i=1}^n w_i x_{i1,r}^{q^*}}{\sum_{i=1}^n w_i} \right)^{1/q^*}$$

$$\le \max_{w_i \in [w_{i1,l}, w_{i1,r}]} \left(\frac{\sum_{i=1}^n w_i x_{i1,r}^{q^*}}{\sum_{i=1}^n w_i} \right)^{1/q^*} = y_{1,r}. \tag{30}$$

So, $\bar{Y}_{\text{LWPM}}$ is convex. In a similar way, we can also show that $\underline{Y}_{\text{LWPM}}$ is convex. Consequently, $\tilde{Y}_{\text{LWPM}}$ is convex and normal.

Next we need to show $f \ge b$ and $g \le c$ in Fig. 10

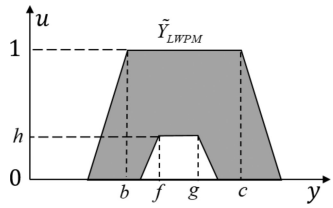

Fig. 10. $\tilde{Y}_{\text{LWPM}}$ in the LWPM. $\tilde{X}_i$ and $\tilde{W}_i$ are shown in Fig. 9(a) and (b), respectively.

$$b = \min_{w_i \in [b_i', c_i']} \left(\frac{\sum_{i=1}^n w_i b_i^{q^*}}{\sum_{i=1}^n w_i} \right)^{1/q^*} \tag{31}$$

$$c = \max_{w_i \in [b_i', c_i']} \left(\frac{\sum_{i=1}^n w_i c_i^{q^*}}{\sum_{i=1}^n w_i} \right)^{1/q^*} \tag{32}$$

$$f = \min_{w_i \in [f_i', g_i']} \left(\frac{\sum_{i=1}^n w_i f_i^{q^*}}{\sum_{i=1}^n w_i} \right)^{1/q^*} \tag{33}$$

$$g = \max_{w_i \in [f_i', g_i']} \left(\frac{\sum_{i=1}^n w_i g_i^{q^*}}{\sum_{i=1}^n w_i} \right)^{1/q^*}. \tag{34}$$

Because z^{1/q^*} increases with z when $q^* > 0$, to show that $f \ge b$ and $g \le c$, we only need to show that

$$\min_{w_i \in [f_i', g_i']} \frac{\sum_{i=1}^n w_i f_i^{q^*}}{\sum_{i=1}^n w_i} \ge \max_{w_i \in [b_i', c_i']} \frac{\sum_{i=1}^n w_i b_i^{q^*}}{\sum_{i=1}^n w_i} \tag{35}$$

$$\min_{w_i \in [f_i', g_i']} \frac{\sum_{i=1}^n w_i g_i^{q^*}}{\sum_{i=1}^n w_i} \le \max_{w_i \in [b_i', c_i']} \frac{\sum_{i=1}^n w_i c_i^{q^*}}{\sum_{i=1}^n w_i} \tag{36}$$

which can be proved similarly as (21) and (22) in the LWA. So, $\tilde{Y}_{\text{LWPM}}$ is a well-shaped IT2 FS. ■

Theorem 8: If all input IT2 FSs are well shaped, then the IT2 FS computed from PR is also well shaped. ■

Proof: There are two types of PR.

[3][28] used $q \to r$; however, r has been used in this paper to denote *right*; to avoid confusion, we use $q \to q^*$ in this paper.

[4][28] states that In the IT2 case, this computation (weighted power mean interval computation) is applied to both the upper and lower bounding functions for the scores and weights to determine the corresponding upper and lower bounding functions of the global score.

1) Firing interval based PR [23], where

$$\tilde{Y}_{\text{FI}} = \frac{\sum_{i=1}^{n} \tilde{X}_i F_i}{\sum_{i=1}^{n} F_i} \tag{37}$$

in which $F_i = [\underline{f}_i, \bar{f}_i]$ is the firing interval of the ith rule. We can view F_i as a special well-shaped IT2 FS $\tilde{F}_i$, where

$$u_{\bar{F}_i}(f) = u_{\underline{F}_i}(f) = \begin{cases} 1, & f \in [\underline{f}_i, \bar{f}_i] \\ 0, & \text{otherwise.} \end{cases} \tag{38}$$

Then, $\tilde{Y}_{\text{FI}}$ in (37) becomes an LWA. It follows from Theorem 4 that $\tilde{Y}_{\text{FI}}$ is a well-shaped IT2 FS.

2) Similarity-based PR [42], where

$$\tilde{Y}_S = \frac{\sum_{i=1}^{n} \tilde{X}_i f_i}{\sum_{i=1}^{n} f_i} \tag{39}$$

in which f_i is the firing level of the ith rule computed from the similarities. Again, we can view f_i as a special well-shaped IT2 FS $\tilde{F}_i$ where

$$u_{\bar{F}_i}(f) = u_{\underline{F}_i}(f) = \begin{cases} 1, & f = f_i \\ 0, & \text{otherwise.} \end{cases} \tag{40}$$

Then, $\tilde{Y}_S$ in (39) becomes an LWA. It follows from Theorem 4 that $\tilde{Y}_S$ is also a well-shaped IT2 FS. ■

III. Constrained Uncertainty Measures of Well-Shaped IT2 FSs Using the CRT

As pointed out by Zadeh [51], uncertainty is an attribute of information. He proposed to use the generalized theory of uncertainty (GTU) to handle it. In GTU, uncertainty is linked to information through the concept of granular structure – a concept which plays a key role in human interaction with the real world [11], [49], [50].

FSs are natural granules in GTU. However, before they can be used in GTU, there is a need to quantify the uncertainty associated with them. Klir [15] states that once uncertainty (and information) measures become well justified, they can very effectively be utilized for managing uncertainty and the associated information. For example, they can be utilized for extrapolating evidence, assessing the strength of relationship between given groups of variables, assessing the influence of given input variables on given output variables, measuring the loss of information when a system is simplified, and the like.

Centroid, cardinality, fuzziness, variance, and skewness are all uncertainty measures for FSs. They have been extensively studied in the literature for T1 FSs. In [38], we defined these five uncertainty measures for arbitrary IT2 FSs based on the Mendel–John RT, and our definitions have been extended to general T2 FSs [53]. In this section, we define and compute them for well-shaped IT2 FSs using the CRT.

A. Constrained Centroid of a Well-Shaped IT2 FS Using the CRT

The centroid $c(A)$ of a T1 FS A is defined as

$$c(A) = \frac{\sum_{i=1}^{N} x_i u_A(x_i)}{\sum_{i=1}^{N} u_A(x_i)}. \tag{41}$$

Definition 5: [38] The (unconstrained) *centroid* $C_{\tilde{A}}$ of an IT2 FS $\tilde{A}$, based on the Mendel–John RT, is the union of the centroids of all its embedded T1 FSs A_e, i.e.,

$$C_{\tilde{A}} \equiv \bigcup_{\forall A_e} c(A_e) = \left[c_l(\tilde{A}), c_r(\tilde{A})\right] \tag{42}$$

where

$$c_l(\tilde{A}) = \min_{\forall A_e} c(A_e) \tag{43}$$

$$c_r(\tilde{A}) = \max_{\forall A_e} c(A_e). \tag{44}$$

■

It has been shown [6], [12], [20], [21], [25] that $c_l(\tilde{A})$ and $c_r(\tilde{A})$ can be expressed as

$$\begin{aligned} c_l(\tilde{A}) &= \min_{k \in [1, N-1]} \frac{\sum_{i=1}^{k} x_i u_{\bar{A}}(x_i) + \sum_{i=k+1}^{N} x_i u_{\underline{A}}(x_i)}{\sum_{i=1}^{k} u_{\bar{A}}(x_i) + \sum_{i=k+1}^{N} u_{\underline{A}}(x_i)} \\ &\equiv \frac{\sum_{i=1}^{L} x_i u_{\bar{A}}(x_i) + \sum_{i=L+1}^{N} x_i u_{\underline{A}}(x_i)}{\sum_{i=1}^{L} u_{\bar{A}}(x_i) + \sum_{i=L+1}^{N} u_{\underline{A}}(x_i)} \end{aligned} \tag{45}$$

$$\begin{aligned} c_r(\tilde{A}) &= \max_{k \in [1, N-1]} \frac{\sum_{i=1}^{k} x_i u_{\underline{A}}(x_i) + \sum_{i=k+1}^{N} x_i u_{\bar{A}}(x_i)}{\sum_{i=1}^{k} u_{\underline{A}}(x_i) + \sum_{i=k+1}^{N} u_{\bar{A}}(x_i)} \\ &\equiv \frac{\sum_{i=1}^{R} x_i u_{\underline{A}}(x_i) + \sum_{i=R+1}^{N} x_i u_{\bar{A}}(x_i)}{\sum_{i=1}^{R} u_{\underline{A}}(x_i) + \sum_{i=R+1}^{N} u_{\bar{A}}(x_i)}. \end{aligned} \tag{46}$$

Switch points L and R, as well as $c_l(\tilde{A})$ and $c_r(\tilde{A})$, can be computed by using the iterative Karnik–Mendel (KM) algorithms [12], [21], or many other more efficient algorithms [34].

Definition 6: The *constrained centroid* $C_{\tilde{A}}^c$ of a well-shaped IT2 FS $\tilde{A}$, based on the CRT, is the union of the centroids of all its convex and normal embedded T1 FSs A_e^{CN}, i.e.,

$$C_{\tilde{A}}^c \equiv \bigcup_{\forall A_e^{CN}} c\left(A_e^{CN}\right) = \left[c_l^c\left(\tilde{A}\right), c_r^c\left(\tilde{A}\right)\right] \tag{47}$$

where

$$c_l^c\left(\tilde{A}\right) = \min_{\forall A_e^{CN}} c\left(A_e^{CN}\right), \quad c_r^c\left(\tilde{A}\right) = \max_{\forall A_e^{CN}} c\left(A_e^{CN}\right). \tag{48}$$

■

Similar to the unconstrained centroid, for $c_l^c(\tilde{A})$, we still need a large weight for small x and a small weight for large x, i.e., the corresponding embedded T1 FS must switch from the UMF to the LMF at some point. However, since this A_e^{CN} must be convex and normal, we have two constraints.

1) Because A_e^{CN} must be normal, at least one point on it must have membership 1. So, the left switch point L^c must satisfy $x_{L^c} \geq b$, where b is the left-most point on the top base of $\bar{A}$, as shown in Fig. 11(a).

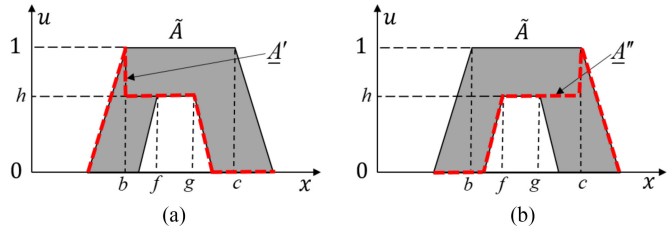

Fig. 11. (a) $\underline{A}'$, the LMF that should be used in the KM algorithm for computing $c_l^c(\tilde{A})$. (b) $\underline{A}''$, the LMF that should be used in the KM algorithm for computing $c_r^c(\tilde{A})$.

2) Because A_e^{CN} must be convex, if the switch point is between b and f, as shown in Fig. 11(a), then the MF of A_e^{CN} between b and f must be raised to h, the height of the LMF, to ensure that it is convex.

Though these two constraints seem complex, they can be simultaneously satisfied by smartly redefining the LMF of $\tilde{A}$ and then using it in the KM algorithm, as explained in the following algorithm for computing $c_l^c(\tilde{A})$.

The algorithm for computing $c_l^c(\tilde{A})$, the left end point of the constrained centroid of a well-shaped IT2 FS:

(1) define

$$u_{\underline{A}'}(x) = \begin{cases} u_{\bar{A}}(x), & x \le b \\ h, & b < x < f \\ u_{\underline{A}}(x), & x \ge f; \end{cases}$$

(2) use $u_{\underline{A}'}(x)$ and $u_{\bar{A}}(x)$ in the KM algorithm to compute $c_l^c(\tilde{A})$.

The motivation for defining $u_{\underline{A}'}(x) = u_{\bar{A}}(x)$ for $x \le b$ is to ensure that b is included in every embedded T1 FS, i.e., every embedded T1 FS is normal.

Similarly, to compute $c_r^c(\tilde{A})$, a small weight should be used for small x and large weight for large x, i.e., the corresponding A_e^{CN} should still switch from the LMF to the UMF at some point. Because A_e^{CN} must be normal, at least one point on it must have membership 1. So, the right switch point R^c must satisfy $x_{R^c} \le c$, where c is the right-most point on the top base of the UMF of $\tilde{A}$, as shown in Fig. 11(b). Again, by smartly redefining the LMF of $\tilde{A}$, the KM algorithm can be used to compute $c_l^c(\tilde{A})$.

The algorithm for computing $c_r^c(\tilde{A})$, the right end point of the constrained centroid of a well-shaped IT2 FS:

1) define

$$u_{\underline{A}''}(x) = \begin{cases} u_{\underline{A}}(x), & x \le f \\ h, & f < x < c \\ u_{\bar{A}}(x), & x \ge c; \end{cases}$$

2) use $u_{\underline{A}''}(x)$ and $u_{\bar{A}}(x)$ in the KM algorithm to compute $c_r^c(\tilde{A})$.

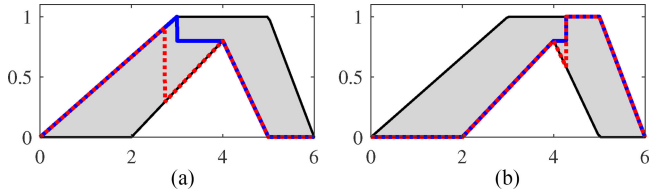

Fig. 12. Embedded T1 FSs determining, (a) $c_l(\tilde{A})$ (red dashed curve) and $c_l^c(\tilde{A})$ (blue solid curve), and (b) $c_r(\tilde{A})$ (red dashed curve) and $c_r^c(\tilde{A})$ (blue solid curve).

The motivation for defining $\underline{u}''_{\tilde{A}}(x) = u_{\bar{A}}(x)$ for $x \ge c$ is to ensure that c is included in every embedded T1 FS, i.e., every embedded T1 FS is normal.

Example 1: Consider the FOU shown in Fig. 12. The domain of x, $[0, 6]$, was discretized into 1000 equally-spaced points in the computation, i.e., $N = 1000$. In this example, $C_{\tilde{A}} = [2.6733, 4.5745]$ and $C_{\tilde{A}}^c = [2.7901, 4.5604]$. Observe that $C_{\tilde{A}}^c \subset C_{\tilde{A}}$, which is intuitive, because $C_{\tilde{A}}^c$ is computed from only a subset of those embedded T1 FSs used to compute $C_{\tilde{A}}$. Also, observe from Fig. 12 that the actual embedded T1 FSs used for computing $C_{\tilde{A}}^c$ and $C_{\tilde{A}}$ are quite different: the embedded T1 FSs for $C_{\tilde{A}}^c$ are convex and normal, but those for $C_{\tilde{A}}$ can be nonconvex and/or subnormal. ■

B. Constrained Cardinality of a Well-Shaped IT2 FS Using the CRT

Definition 7: [38] The *normalized cardinality* of a T1 FS A is defined as

$$p(A) = \frac{|X|}{N} \sum_{i=1}^{N} u_A(x_i) \tag{49}$$

where $|X| = x_N - x_1$ is the length of the universe of discourse used in the computation. ■

Definition 8: [38] The (unconstrained) cardinality of an IT2 FS $\tilde{A}$, based on the Mendel–John RT, is the union of normalized cardinalities of all its embedded T1 FSs A_e, i.e.,

$$P_{\tilde{A}} \equiv \bigcup_{\forall A_e} p(A_e) = \left[p_l\left(\tilde{A}\right), p_r\left(\tilde{A}\right) \right] \tag{50}$$

where

$$p_l\left(\tilde{A}\right) = \min_{\forall A_e} p(A_e), \quad p_r\left(\tilde{A}\right) = \max_{\forall A_e} p(A_e). \tag{51}$$

■

In [38] we have shown that $p_l(\tilde{A})$ and $p_r(\tilde{A})$ can be computed as

$$p_l(\tilde{A}) = p(\underline{A}) \tag{52}$$

$$p_r(\tilde{A}) = p(\bar{A}). \tag{53}$$

Definition 9: The *constrained cardinality* of a well-shaped IT2 FS $\tilde{A}$, based on the CRT, is the union of normalized cardinalities of all its convex and normal embedded

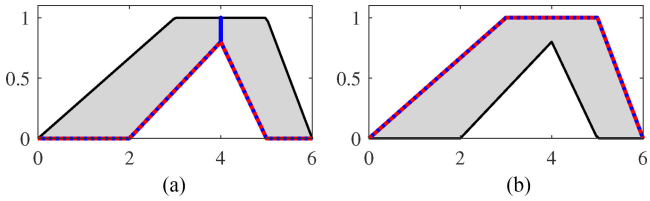

Fig. 13. Embedded T1 FSs determining, (a) $p_l(\tilde{A})$ (red dashed curve) and $p_l^c(\tilde{A})$ (blue solid curve), and (b) $p_r(\tilde{A})$ (red dashed curve) and $p_r^c(\tilde{A})$ (blue solid curve).

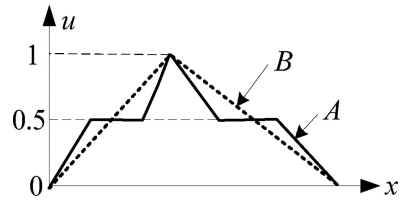

Fig. 14. A (solid lines) is more fuzzy than B (dashed lines).

T1 FSs A_e^{CN}, i.e.,

$$P_{\tilde{A}}^c \equiv \bigcup_{\forall A_e^{CN}} p\left(A_e^{CN}\right) = \left[p_l^c\left(\tilde{A}\right), p_r^c\left(\tilde{A}\right)\right] \tag{54}$$

where

$$p_l^c\left(\tilde{A}\right) = \min_{\forall A_e^{CN}} p\left(A_e^{CN}\right) \tag{55}$$

$$p_r^c\left(\tilde{A}\right) = \max_{\forall A_e^{CN}} p\left(A_e^{CN}\right). \tag{56}$$

■

Observe that $\bar{A}$ in (53) is already convex and normal; so, $p_r^c(\tilde{A}) = p_r(\tilde{A}) = p(\bar{A})$. However, $\underline{A}$ in (52) is generally not normal. So, generally $p_l^c(\tilde{A}) \neq p_l(\tilde{A})$.

Theorem 9: $p_l^c(\tilde{A})$ in (55) is the cardinality of a minimally modified convex and normal embedded T1 FS from $\underline{A}$, by bringing any single point on its top base to membership 1 and keeping all other points untouched. ■

Proof: As shown in [38], the LMF $\underline{A}$ of a well-shaped IT2 FS $\tilde{A}$ [an example is shown in Fig. 13(a)] has the smallest cardinality among all the embedded T1 FSs. It is convex, but generally subnormal. We need to bring at least one point on $\underline{A}$ to membership 1 to make it normal. At the same time, we need to make sure this modification introduces the smallest increase to the cardinality of $\underline{A}$. Clearly, this can be achieved by bringing any single point on its top base to membership 1 and keeping all other points untouched, because the points on the top base are the closest to membership 1. ■

Consequently, the following procedure can be used to compute $P_{\tilde{A}}^c$.

The algorithm for computing $P_{\tilde{A}}^c = \left[p_l^c(\tilde{A}), p_r^c(\tilde{A})\right]$, the constrained cardinality of a well-shaped IT2 FS:

1) $p_l^c(\tilde{A}) = p(\underline{A}) + \frac{|X|}{N}(1-h)$, where h is the height of the LMF;
2) $p_r^c(\tilde{A}) = p(\bar{A})$, which equals the cardinality of the UMF.

Note that when computing $p_l^c(\tilde{A})$ in the continuous space, the modification to $\underline{A}$ may not be reflected numerically, as $\lim_{N\to\infty} \frac{|X|}{N}(1-h) = 0$. However, theoretically there should be a "spike" at the top of $\underline{A}$ in computing $p_l^c(\tilde{A})$.

Example 2: For the IT2 FS $\tilde{A}$ shown in Fig. 13, which is the same as the one shown in Fig. 12, $P_{\tilde{A}} = [0.7992, 3.9960]$ and $P_{\tilde{A}}^c = [0.8004, 3.9960]$. Observe that $P_{\tilde{A}}^c \subset P_{\tilde{A}}$. ■

C. Constrained Fuzziness (Entropy) of a Well-Shaped IT2 FS Using the CRT

The fuzziness (entropy) of a T1 FS is used to quantify the amount of vagueness in it. A T1 FS C is most fuzzy when all its memberships equal 0.5. A T1 FS A is more fuzzy than a T1 FS B if A is nearer to such a C than B is. For example, in Fig. 14 A is more fuzzy than B because the memberships of A are closer to $u = 0.5$.

Different fuzziness measures have been proposed [13] for T1 FSs. In this paper, we use the following *general fuzziness measure* [16].

Definition 10: [16] A *general fuzziness measure* of a T1 FS A, $f(A)$, is defined as

$$f(A) = h\left(\sum_{i=1}^{N} g(u_A(x_i))\right) \tag{57}$$

where h is a monotonically increasing function from R^+ to R^+, and, $g : [0,1] \to R^+$ is a function associated with each x_i. Additionally, 1) $g(0) = g(1) = 0$; 2) $g(0.5)$ is a unique maximum of g; and 2) g must be monotonically increasing on $[0, 0.5]$ and monotonically decreasing on $[0.5, 1]$. ■

Theoretically, $f(A)$ can be any T1 fuzziness definition satisfying the requirements in Definition 10; however, we prefer a normalized version such as Yager's definition [47]

$$f_{_Y}(A) = 1 - \frac{\left[\sum_{i=1}^{N} |2u_A(x_i) - 1)|^{\beta}\right]^{\frac{1}{\beta}}}{N^{\frac{1}{\beta}}} \tag{58}$$

where β is a positive constant, because it converges as N increases.

Several researchers have proposed definitions of the fuzziness for IT2 FSs [2], [4], [30], [32], [38], [52]. The most popular one is Wu and Mendel's interval fuzziness definition.

Definition 11: [38] The (unconstrained) *fuzziness* $F_{\tilde{A}}$ of an IT2 FS $\tilde{A}$, based on the Mendel–John RT, is the union of the fuzziness of all its embedded T1 FSs A_e, i.e.,

$$F_{\tilde{A}} \equiv \bigcup_{\forall A_e} f(A_e) = \left[f_l\left(\tilde{A}\right), f_r\left(\tilde{A}\right)\right] \tag{59}$$

where $f_l(\tilde{A})$ and $f_r(\tilde{A})$ are the minimum and maximum of the fuzziness of all A_e, respectively, i.e.,

$$f_l\left(\tilde{A}\right) = \min_{\forall A_e} f(A_e) \tag{60}$$

$$f_r\left(\tilde{A}\right) = \max_{\forall A_e} f(A_e) \tag{61}$$

and $f(A_e)$ satisfies Definition 3. ■

The unconstrained fuzziness of an IT2 FS is computed by the following theorem.

Theorem 10: [38] Let A_{e1} be defined as

$$u_{A_{e1}}(x) = \begin{cases} u_{\bar{A}}(x), & |u_{\bar{A}}(x) - 0.5| > |u_{\underline{A}}(x) - 0.5| \\ u_{\underline{A}}(x), & |u_{\bar{A}}(x) - 0.5| \leq |u_{\underline{A}}(x) - 0.5| \end{cases} \tag{62}$$

and A_{e2} be defined as

$$u_{A_{e2}}(x) = \begin{cases} u_{\bar{A}}(x), & u_{\bar{A}}(x) < 0.5, u_{\underline{A}}(x) < 0.5 \\ u_{\underline{A}}(x), & u_{\bar{A}}(x) > 0.5, u_{\underline{A}}(x) > 0.5 \\ 0.5, & \text{otherwise.} \end{cases} \tag{63}$$

Then (60) and (61) can be computed as

$$f_l\left(\tilde{A}\right) = f(A_{e1}) \tag{64}$$

$$f_r\left(\tilde{A}\right) = f(A_{e2}) \tag{65}$$

where $f(A)$ is defined in (57). ■

In this paper, we define the constrained fuzziness of a well-shaped IT2 FS as follows.

Definition 12: The *constrained fuzziness* $F_{\tilde{A}}^c$ of a well-shaped IT2 FS $\tilde{A}$, based on the CRT, is the union of the fuzziness of all its convex and normal embedded T1 FSs A_e^{CN}, i.e.,

$$F_{\tilde{A}}^c \equiv \bigcup_{\forall A_e^{CN}} f(A_e^{CN}) = \left[f_l^c\left(\tilde{A}\right), f_r^c\left(\tilde{A}\right)\right], \tag{66}$$

where

$$f_l^c(\tilde{A}) = \min_{\forall A_e^{CN}} f(A_e^{CN}) \tag{67}$$

$$f_r^c(\tilde{A}) = \max_{\forall A_e^{CN}} f(A_e^{CN}). \tag{68}$$

■

The following two theorems show how the constrained fuzziness of a well-shaped IT2 FS can be computed.

Theorem 11: $f_l^c(\tilde{A})$ in (67) is the same as $f_l(\tilde{A})$ in (64). ■

Proof: $f_l(\tilde{A})$ in (64) is the smallest fuzziness of all possible embedded T1 FSs, no matter convex or not, or normal or not. We only need to show that the corresponding A_{e1} in (62) is convex and normal. Then it follows that $f_l^c(\tilde{A}) = f_l(\tilde{A}) = f(A_{e1})$.

Let x' be the solution that

$$u_{\bar{A}}(x') - 0.5 = 0.5 - u_{\underline{A}}(x') \tag{69}$$

i.e., $u_{\bar{A}}(x')$ and $u_{\underline{A}}(x')$ are at the same distance to membership 0.5. (69) is equivalent to

$$u_{\underline{A}}(x') + u_{\bar{A}}(x') = 1. \tag{70}$$

Generally the solution of x' consists of two intervals, $[x'_{l,1}, x'_{l,2}]$ and $[x'_{r,1}, x'_{r,2}]$. $[x'_{r,1}, x'_{r,2}] \subseteq [g, d]$ in Fig. 15, because

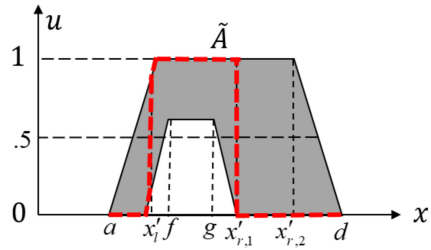

Fig. 15. Illustration of A_{e1} (the red dashed curve).

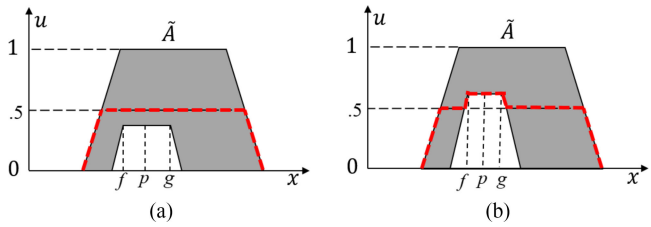

Fig. 16. Illustration of A_{e2} (red dashed curve) for different heights of the LMF.

$u_{\underline{A}}(g) + u_{\bar{A}}(g) > 1$, $u_{\underline{A}}(d) + u_{\bar{A}}(d) = 0$, and $u_{\underline{A}}(x) + u_{\bar{A}}(x)$ is nonincreasing in $[g, d]$ according to the definition of a well-shaped IT2 FS. Similarly, we can show $[x'_{l,1}, x'_{l,2}] \subseteq [a, f]$, and Fig. 15 shows a special case that $x'_{l,1} = x'_{l,2} = x'_l$.

Then according to (62), A_{e1} is the red dashed curve in Fig. 15, i.e., it first stays on the LMF, then switches to the UMF at $x = x'_{l,2}$, and then switches back to the LMF at $x = x'_{r,1}$. Clearly, A_{e1} is convex and normal. This completes the proof. ■

Theorem 12: $f_r^c(\tilde{A})$ in (68) is the fuzziness of a minimally modified convex and normal embedded T1 FS from A_{e2} in (63), by bringing any single point on its top base to membership 1 and keeping all other points untouched. ■

Proof: A_{e2} defined in (63) of a well-shaped IT2 FS $\tilde{A}$ has the largest fuzziness. It is convex, but generally subnormal, as shown in Fig. 16. We need to bring one point on A_{e2} to membership 1 to make it normal, but at the same time, keep it convex and minimize the reduction to its fuzziness.

Consider $x = p \in [f, g]$, as shown in Fig. 16. Then, according to the definition of a well-shaped IT2 FS, $u_{\bar{A}}(p) = 1$. If $u_{\underline{A}}(x) \leq 0.5$, as shown in Fig. 16(a), then according to the definition of A_{e2} in (63), $u_{A_{e2}}(p) = 0.5$, i.e., every point on the top base of A_{e2} has membership 0.5. We can bring any such point to membership 1 to make the modified A_{e2} normal and convex. At the same time, because the points on the top base of A_{e2} are closest to membership 1, this introduces the minimum decrease to its fuzziness. Note that we cannot choose a point not on the top base because then the modified A_{e2} is nonconvex.

On the other hand, if $u_{\underline{A}}(x) > 0.5$, as shown in Fig. 16(b), then according to the definition of A_{e2} in (63), $u_{A_{e2}}(p) = u_{\underline{A}}(p)$. Again, we can bring $(p, u_{A_{e2}}(p))$ to membership 1 to make the modified A_{e2} normal and convex. Because $(p, u_{A_{e2}}(p))$ is the closest point on A_{e2} to membership 1, this introduces the minimum decrease to its fuzziness. ■

In summary, the following procedure can be used to compute the constrained fuzziness of a well-shaped IT2 FS.

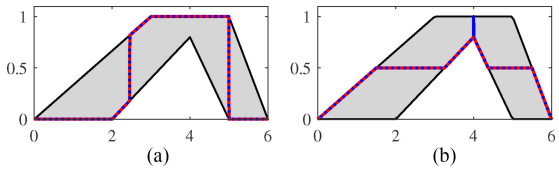

Fig. 17. Embedded T1 FSs determining, (a) $f_l(\tilde{A})$ (red dashed curve) and $f_l^c(\tilde{A})$ (blue solid curve), and (b) $f_r(\tilde{A})$ (red dashed curve) and $f_r^c(\tilde{A})$ (blue solid curve).

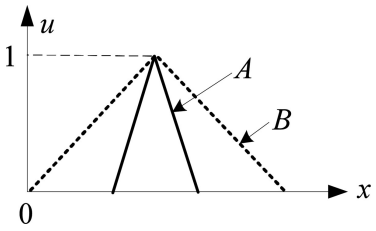

Fig. 18. Illustration of the variance of T1 FSs.

The algorithm for computing $F_{\tilde{A}}^c = \left[f_l^c(\tilde{A}), f_r^c(\tilde{A})\right]$, the constrained fuzziness of a well-shaped IT2 FS:

1) $f_l^c(\tilde{A}) = f_l(\tilde{A}) = f(A_{e1})$, where A_{e1} is defined in (62);
2) $f_r^c(\tilde{A}) = f(A_{e3})$, where $A_{e3} = A_{e2}$ in (63), except that a single $x \in [f, g]$ on A_{e2} is modified to have membership 1.

Note that when computing $f_r^c(\tilde{A})$ in the continuous space, the modification to A_{e2} may not be reflected numerically, as the integral on the "spike" is zero. However, theoretically there should be a "spike" at the top of A_{e2} in computing $f_r^c(\tilde{A})$.

Example 3: Consider the IT2 FS $\tilde{A}$ in Fig. 17 , which is the same as the IT2 FS shown in Fig. 12. According to (62) and (63), A_{e1} and A_{e2} are as shown in Fig. 17(a) and (b), respectively, as the red dashed curve. When Yager's definition is used and $\beta = 1$, $F_{\tilde{A}} = [0.0303, 0.7763]$, and $F_{\tilde{A}}^c = [0.0303, 0.7759]$. Observe that $F_{\tilde{A}}^c \subset F_{\tilde{A}}$. ■

D. Variance of an IT2 FS

The variance of a T1 FS A measures its compactness, i.e., a smaller (larger) variance means A is more (less) compact. For example, in Fig. 18, A has smaller variance than B because it is more compact.

There are different definitions of the variance of a T1 FS [3], [17]. In this paper, we use the following *relative variance* of A_e to $\tilde{A}$ [38].

Definition 13: [38] The *relative variance* of an embedded T1 FS A_e to an IT2 FS $\tilde{A}$, $v_{\tilde{A}}(A_e)$, is defined as

$$v_{\tilde{A}}(A_e) = \frac{\sum_{i=1}^{N}\left[x_i - c\left(\tilde{A}\right)\right]^2 \mu_{A_e}(x_i)}{\sum_{i=1}^{N}\mu_{A_e}(x_i)} \tag{71}$$

where

$$c\left(\tilde{A}\right) = \frac{c_l\left(\tilde{A}\right) + c_r\left(\tilde{A}\right)}{2} \tag{72}$$

is the center of the centroid of $\tilde{A}$, $C_{\tilde{A}}$, that is given in (42). ■

Definition 14: [38] The *variance* of an IT2 FS $\tilde{A}$, $V_{\tilde{A}}$, is the union of relative variance of all its embedded T1 FSs A_e, i.e.,

$$V_{\tilde{A}} \equiv \bigcup_{\forall A_e} v_{\tilde{A}}(A_e) = \left[v_l\left(\tilde{A}\right), v_r\left(\tilde{A}\right)\right] \tag{73}$$

where $v_l(\tilde{A})$ and $v_r(\tilde{A})$ are the minimum and maximum relative variance of all A_e, respectively, i.e.,

$$v_l\left(\tilde{A}\right) = \min_{\forall A_e} v_{\tilde{A}}(A_e) \tag{74}$$

$$v_r\left(\tilde{A}\right) = \max_{\forall A_e} v_{\tilde{A}}(A_e). \tag{75}$$

■

The iterative KM Algorithms can be used to compute $v_l(\tilde{A})$ and $v_r(\tilde{A})$ [38].

In this paper, we define the constrained variance of a well-shaped IT2 FS as follows.

Definition 15: The *constrained variance* $V_{\tilde{A}}^c$ of a well-shaped IT2 FS $\tilde{A}$, based on the CRT, is the union of the relative variance of all its convex and normal embedded T1 FSs A_e^{CN}, i.e.,

$$V_{\tilde{A}}^c \equiv \bigcup_{\forall A_e^{CN}} v_{\tilde{A}}\left(A_e^{CN}\right) = \left[v_l^c\left(\tilde{A}\right), v_r^c\left(\tilde{A}\right)\right] \tag{76}$$

where

$$v_l^c\left(\tilde{A}\right) = \min_{\forall A_e^{CN}} v_{\tilde{A}}\left(A_e^{CN}\right) \tag{77}$$

$$v_r^c\left(\tilde{A}\right) = \max_{\forall A_e^{CN}} v_{\tilde{A}}\left(A_e^{CN}\right). \tag{78}$$

■

The computation of the constrained variance is much more complicated that the constrained centroid/cardinality/fuzziness, and we do not have a closed-form solution for it. So, the following algorithm is used to compute $v_l^c(\tilde{A})$ and $v_r^c(\tilde{A})$, by minimally modifying the corresponding A_e in computing $v_l(\tilde{A})$ and $v_r(\tilde{A})$.

The algorithm for computing $V_{\tilde{A}}^c = \left[v_l^c(\tilde{A}), v_r^c(\tilde{A})\right]$, the constrained variance of a well-shaped IT2 FS.

1) For $v_l^c(\tilde{A})$:
   a) use the KM algorithm to compute $v_l(\tilde{A})$, and identify the corresponding A_e;
   b) if A_e is not already normal, then minimally modify it to make it normal;
   c) if A_e is not already convex, then minimally modify it to make it convex.
2) For $v_r^c(\tilde{A})$:
   a) use the KM algorithm to compute $v_r(\tilde{A})$, and identify the corresponding A_e;
   b) if A_e is not already normal, then minimally modify it to make it normal;
   c) if A_e is not already convex, then minimally modify it to make it convex.

To minimally modify a subnormal A_e to make it normal, we pick a point on A_e that is also on $\tilde{A}$ and is closest to either

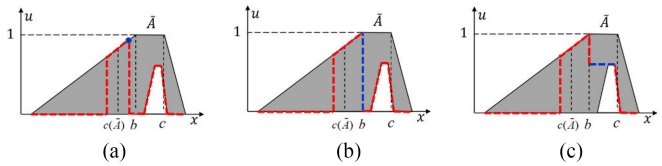

Fig. 19. Procedure to compute $v_l^c(\tilde{A})$. (a) A_e for computing $v_l(\tilde{A})$. (b) Minimal modification to make A_e normal. (c) Minimal modification to make A_e convex.

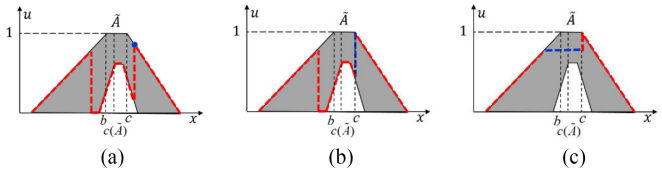

Fig. 20. Procedure to compute $v_r^c(\tilde{A})$. (a) A_e for computing $v_r(\tilde{A})$. (b) Minimal modification to make A_e normal. (c) Minimal modification to make A_e convex.

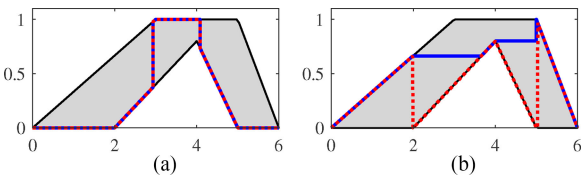

Fig. 21. Embedded T1 FSs determining, (a) $v_l(\tilde{A})$ (red dashed curve) and $v_l^c(\tilde{A})$ (blue solid curve), and (b) $v_r(\tilde{A})$ (red dashed curve) and $v_r^c(\tilde{A})$ (blue solid curve).

$(b,1)$ or $(c,1)$ on the top base of $\bar{A}$ (for example, the blue point in Fig. 19(a) for $v_l^c(\tilde{A})$, and the blue point in Fig. 20(a) for $v_r^c(\tilde{A})$), and then bring it to $(b,1)$ or $(c,1)$, whichever is closer (for example, Fig. 19(b) for $v_l^c(\tilde{A})$, and Fig. 20(b) for $v_r^c(\tilde{A})$).

To minimally modify a nonconvex A_e to make it convex, we first compute

$$h_1 = \max_{x'<x} u(x'), \quad h_2 = \max_{x'>x} u(x') \tag{79}$$

and then change $u(x)$ to $\min(h_1, h_2)$ if $u(x) < h_1$ and $u(x) < h_2$. Usually most $u(x)$ will remain unchanged, as shown in Fig. 19(c) for $v_l^c(\tilde{A})$ and Fig. 20(c) for $v_r^c(\tilde{A})$.

Example 4: Consider the IT2 FS $\tilde{A}$ in Fig. 21, which is the same as the IT2 FS shown in Fig. 12. We have $V_{\tilde{A}} = [0.3301, 2.3215]$ and $V_{\tilde{A}}^c = [0.3301, 2.0031]$. Observe that $V_{\tilde{A}}^c \subset V_{\tilde{A}}$. ■

E. Skewness of an IT2 FS

The *skewness* of a T1 FS A, $s(A)$, is an indicator of its symmetry. For example in Fig. 22, A has skewness smaller than zero because it skews to the right, B has skewness larger than zero because it skews to the left, and C has skewness zero because it is symmetrical.

There are different definitions of skewness for T1 FSs [1], [29], [37]. In this paper, we use the following *relative skewness* of A_e to $\tilde{A}$ [38].

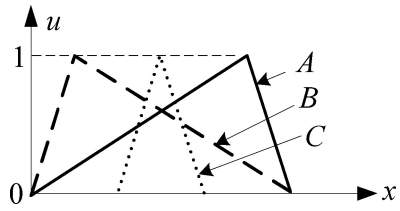

Fig. 22. Illustration of the skewness of T1 FSs.

Definition 16: The *relative skewness* of an embedded T1 FS A_e to an IT2 FS $\tilde{A}$, $s_{\tilde{A}}(A_e)$, is defined as

$$s_{\tilde{A}}(A_e) = \frac{\sum_{i=1}^{N}\left[x_i - c\left(\tilde{A}\right)\right]^3 \mu_{A_e}(x_i)}{\sum_{i=1}^{N}\mu_{A_e}(x_i)} \tag{80}$$

where $c(\tilde{A})$ is the center of the centroid of $\tilde{A}$ [see (72)]. ■

Definition 17: The *skewness* of an IT2 FS $\tilde{A}$, $S_{\tilde{A}}$, is the union of the relative skewness of all its embedded T1 FSs A_e, i.e.,

$$S_{\tilde{A}} \equiv \bigcup_{\forall A_e} s_{\tilde{A}}(A_e) = \left[s_l\left(\tilde{A}\right), s_r\left(\tilde{A}\right)\right] \tag{81}$$

where $s_l(\tilde{A})$ and $s_r(\tilde{A})$ are the minimum and maximum relative skewness of all A_e, respectively, i.e.,

$$s_l\left(\tilde{A}\right) = \min_{\forall A_e} s_{\tilde{A}}(A_e) \tag{82}$$

$$s_r\left(\tilde{A}\right) = \max_{\forall A_e} s_{\tilde{A}}(A_e). \tag{83}$$

■

The iterative KM Algorithms can also be used to compute $s_l(\tilde{A})$ and $s_r(\tilde{A})$ [38].

The computation of the constrained skewness is also much more complicated that the constrained centroid/cardinality/fuzziness, and we do not have a closed-form solution for it. So, the following algorithm is used to compute $s_l^c(\tilde{A})$ and $s_r^c(\tilde{A})$, by minimally modifying the corresponding A_e in computing $s_l(\tilde{A})$ and $s_r(\tilde{A})$.

The algorithm for computing $S_{\tilde{A}}^c = \left[s_l^c(\tilde{A}), s_r^c(\tilde{A})\right]$, the constrained variance of a well-shaped IT2 FS.

1) For $s_l^c(\tilde{A})$:
   a) use the KM algorithm to compute $s_l(\tilde{A})$, and identify the corresponding A_e;
   b) if A_e is not already normal, then minimally modify it to make it normal;
   c) if A_e is not already convex, then minimally modify it to make it convex.
2) For $s_r^c(\tilde{A})$:
   a) use the KM algorithm to compute $s_r(\tilde{A})$, and identify the corresponding A_e;
   b) if A_e is not already normal, then minimally modify it to make it normal;
   c) if A_e is not already convex, then minimally modify it to make it convex.

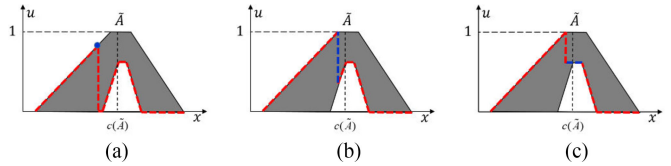

Fig. 23. Procedure to compute $s_l^c(\tilde{A})$. (a) A_e for computing $s_l(\tilde{A})$. (b) Minimal modification to make A_e normal. (c) Minimal modification to make A_e convex.

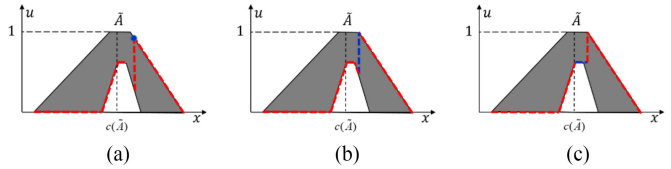

Fig. 24. Procedure to compute $s_r^c(\tilde{A})$. (a) A_e for computing $s_r(\tilde{A})$. (b) Minimal modification to make A_e normal. (c) Minimal modification to make A_e convex.

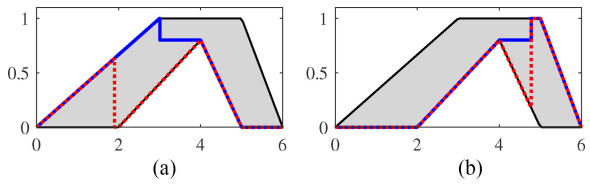

Fig. 25. Embedded T1 FSs determining, (a) $s_l(\tilde{A})$ (red dashed curve) and $s_l^c(\tilde{A})$ (blue solid curve), and (b) $s_r(\tilde{A})$ (red dashed curve) and $s_r^c(\tilde{A})$ (blue solid curve).

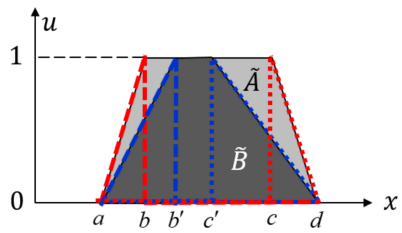

Fig. 26. Completely filled-in $\tilde{A}$ and $\tilde{B}$, and the corresponding embedded T1 FSs used by the CRT to compute their centroids.

The procedures for minimally modifying a subnormal A_e to make it normal, and for minimally modifying a nonconvex A_e to make it convex, are the same as those in the previous subsection. Illustrative examples for $s_l^c(\tilde{A})$ and $s_r^c(\tilde{A})$ are shown in Figs. 23 and 24, respectively.

Example 5: Consider the IT2 FS $\tilde{A}$ in Fig. 25 , which is the same as the IT2 FS shown in Fig. 12. We have $S_{\tilde{A}} = [-4.1481, 2.0321]$ and $S_{\tilde{A}}^c = [-3.1735, 1.9299]$. Observe that $S_{\tilde{A}}^c \subset S_{\tilde{A}}$. ■

IV. Advantages and Limitations of the CRT

The Mendel–John RT [22] has been widely used to compute the centroid of IT2 FSs. However, its output may be counter intuitive for completely filled-in FOUs, as shown in Fig. 26.

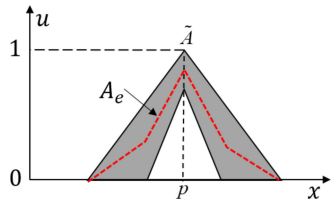

Fig. 27. Homotopic embedded T1 FS of $\tilde{A}$.

When the Mendel–John RT is used, $C_{\tilde{A}} = [a, d] = C_{\tilde{B}}$, which is counter intuitive. In contrast, the CRT gives $C_{\tilde{A}}^c = [c_l, c_r] \subset [a, d]$, where c_l is the centroid of the red dashed T1 FS in Fig. 26, and c_r is the centroid of the red dotted T1 FS. Similarly, the CRT gives $C_{\tilde{B}}^c = [c_l', c_r'] \subset [a, d]$, where c_l' is the centroid of the blue dashed T1 FS in Fig. 26, and c_r' is the centroid of the blue dotted T1 FS. We have $C_{\tilde{B}}^c \subset C_{\tilde{A}}^c$, which is more reasonable than the Mendel–John RT result.

The FOU of an IT2 FS may also be completely covered by homotopic embedded T1 FSs of the LMF and the UMF, i.e., $A_e^\lambda = \lambda\bar{A} + (1-\lambda)\underline{A}$, $\alpha \in [0, 1]$. However, when both $\bar{A}$ and $\underline{A}$ are symmetric about $x = p$, as shown in Fig. 27, A_e^λ is always symmetric about $x = p$ regardless of λ. So, the centroid of A_e^λ is always p, and the centroid of $\tilde{A}$ becomes a single number p, which is counter intuitive. Additionally, most A_e are subnormal. The CRT does not have these problems.

Finally, we need to point out a limitation of the CRT. In a Mamdani IT2 fuzzy logic system [21] that combines the fired rules by using the union, the resulting FOU will be subnormal and nonconvex, so the CRT cannot be applied. In contrast, the Mendel–John RT can accommodate this. Nevertheless, we suggest that the main applications of the CRT should be computing with words [24], as we have shown in Section II-C that IT2 FSs constructed from three different word encoding approaches (IA, EIA, and HMA) are well shaped, and IT2 FSs output by the perceptual computer with four different computing with words engines (LWAs, OLWAs, LWPMs, and PR), are also well shaped.

V. Conclusion

The Mendel–John RT has been widely used in developing many theoretical results for IT2 FSs, including uncertainty measures, similarity measures, subsethood measures, LWAs, OLWAs, LWPMs, and so on. Nonconvex and/or subnormal embedded T1 FSs are included in such RT, whereas in practice, we almost always use only convex and normal FSs. In this paper, we have proposed a CRT for well-shaped IT2 FSs, and shown that IT2 FSs generated by three different word encoding approaches (IA, EIA, and HMA) and four different computing with words engines (LWA, OLWA, LWPM, and PR) are all well-shaped IT2 FSs. We have also proposed algorithms for computing the constrained centroid, cardinality, fuzziness, variance and skewness of well-shaped IT2 FSs based on the CRT. These measures can be used to extend the principles of uncertainty [10], [14] from T1 FSs to IT2 FSs, and to compute the similarity of two well-shaped IT2 FSs [40].

Our future research will compare the constrained uncertainty measures with the unconstrained ones in such applications and investigate which category is more favorable. Additionally, we will extend the CRT from IT2 FSs to general T2 FSs.

REFERENCES

[1] P. P. Bonissone, "A fuzzy sets based linguistic approach: Theory and applications," in *Proc. 12th Winter Simul. Conf.*, Orlando, FL, USA, 1980, pp. 99–111.

[2] P. Burillo and H. Bustince, "Entropy on intuitionistic fuzzy sets and on interval-valued fuzzy sets," *Fuzzy Sets Syst.*, vol. 78, pp. 305–316, 1996.

[3] C. Carlsson and R. Fullér, "On possibilistic mean value and variance of fuzzy numbers," *Fuzzy Sets Syst.*, vol. 122, pp. 315–326, 2001.

[4] C. Cornelis and E. Kerre, "Inclusion measures in intuitionistic fuzzy set theory," *Lecture Notes Comput. Sci.*, vol. 2711, pp. 345–356, 2004.

[5] T. Dereli, A. Baykasoglu, K. Altun, A. Durmusoglu, and I. B. Turksen, "Industrial applications of type-2 fuzzy sets and systems: A concise review," *Comput. Industry*, vol. 62, pp. 125–137, 2011.

[6] K. Duran, H. Bernal, and M. Melgarejo, "Improved iterative algorithm for computing the generalized centroid of an interval type-2 fuzzy set," in *Proc. Annu. Meeting North Amer. Fuzzy Inf. Process. Soc.*, New York, NY, USA, 2008, pp. 1–5.

[7] H. Hagras, "Type-2 FLCs: A new generation of fuzzy controllers," *IEEE Comput. Intell. Mag.*, vol. 2, no. 1, pp. 30–43, Feb. 2007.

[8] H. Hagras and C. Wagner, "Towards the wide spread use of type-2 fuzzy logic systems in real world applications," *IEEE Comput. Intell. Mag.*, vol. 7, no. 3, pp. 14–24, Aug. 2012.

[9] M. Hao and J. M. Mendel, "Encoding words into normal interval type-2 fuzzy sets: HM approach," *IEEE Trans. Fuzzy Syst.*, vol. 24, no. 4, pp. 865–879, Aug. 2016.

[10] D. Harmanec, *Measures of Uncertainty and Information*. [Online]. Available: http://www.sipta.org/documentation/summary_measures/main.html

[11] M. Higashi and G. Klir, *Measures of Uncertainty and Information Based on Possibility Distributions* (Fuzzy Sets for Intelligent Systems). San Mateo, CA, USA: Morgan Kaufmann Publishers, 1993, pp. 217–232.

[12] N. N. Karnik and J. M. Mendel, "Centroid of a type-2 fuzzy set," *Inf. Sci.*, vol. 132, pp. 195–220, 2001.

[13] G. J. Klir and T. A. Folger, *Fuzzy Sets, Uncertainty, and Information*. Englewood Cliffs, NJ, USA: Prentice Hall, 1988.

[14] G. J. Klir and B. Yuan, *Fuzzy Sets and Fuzzy Logic: Theory and Applications*. Upper Saddle River, NJ, USA: Prentice-Hall, 1995.

[15] G. J. Klir, "Principles of uncertainty: What are they? Why do we need them?" *Fuzzy Sets Syst.*, vol. 74, pp. 15–31, 1995.

[16] J. Knopfmacher, "On measures of fuzziness," *J. Math. Anal. Appl.*, vol. 49, pp. 529–534, 1975.

[17] E. Lee and R. Li, "Comparison of fuzzy numbers based on the probability measure of fuzzy events," *Comput. Math. Appl.*, vol. 15, pp. 887–896, 1988.

[18] F. Liu and J. M. Mendel, "Aggregation using the fuzzy weighted average, as computed using the Karnik-Mendel Algorithms," *IEEE Trans. Fuzzy Syst.*, vol. 12, no. 1, pp. 1–12, Feb. 2008.

[19] F. Liu and J. M. Mendel, "Encoding words into interval type-2 fuzzy sets using an interval approach," *IEEE Trans. Fuzzy Syst.*, vol. 16, no. 6, pp. 1503–1521, Dec. 2008.

[20] M. Melgarejo, "A fast recursive method to compute the generalized centroid of an interval type-2 fuzzy set," in *Proc. Annu. Meeting North Amer. Fuzzy Inf. Process. Soc.*, San Diego, CA, USA, 2007, pp. 190–194.

[21] J. Mendel, *Uncertain Rule-based Fuzzy Systems: Introduction and New Directions*, 2nd ed. New York, NY, USA: Springer, 2017.

[22] J. M. Mendel and R. I. John, "Type-2 fuzzy sets made simple," *IEEE Trans. Fuzzy Syst.*, vol. 10, no. 2, pp. 117–127, Apr. 2002.

[23] J. M. Mendel and D. Wu, "Perceptual reasoning for perceptual computing," *IEEE Trans. Fuzzy Syst.*, vol. 16, no. 6, pp. 1550–1564, Dec. 2008.

[24] J. M. Mendel and D. Wu, *Perceptual Computing: Aiding People in Making Subjective Judgments*. Hoboken, NJ, USA: Wiley-IEEE Press, 2010.

[25] J. M. Mendel and H. Wu, "New results about the centroid of an interval type-2 fuzzy set, including the centroid of a fuzzy granule," *Inf. Sci.*, vol. 177, pp. 360–377, 2007.

[26] H. T. Nguyen and V. Kreinovich, "Computing degrees of subsethood and similarity for interval-valued fuzzy sets: Fast algorithms," in *Proc. 9th Int. Conf. Intell. Technol.*, Samui, Thailand, Oct. 2008, pp. 47–55.

[27] J. T. Rickard, J. Aisbett, and G. Gibbon, "Fuzzy subsethood for fuzzy sets of type-2 and generalized type-n," *IEEE Trans. Fuzzy Syst.*, vol. 17, no. 1, pp. 50–60, Feb. 2009.

[28] J. Rickard, J. Aisbett, R. Yager, and G. Gibbon, "Linguistic weighted power means, comparison with the linguistic weighted average," in *Proc. IEEE Int. Conf. Fuzzy Syst.*, Taipei, Taiwan, Jun. 2011, pp. 2185–2192.

[29] P. Subasic and M. Nakatsuyama, "A new representational framework for fuzzy sets," in *Proc. IEEE Int. Conf. Fuzzy Syst.*, Catalonia, Spain, Jul. 1997, pp. 1601–1606.

[30] E. Szmidt and J. Kacprzyk, "Entropy for intuitionistic fuzzy sets," *Fuzzy Sets Syst.*, vol. 118, pp. 467–477, 2001.

[31] K. Tai, A.-R. El-Sayed, M. Biglarbegian, C. I. Gonzalez, O. Castillo, and S. Mahmud, "Review of recent type-2 fuzzy controller applications," *Algorithms*, vol. 9, no. 2, p. 39, 2016.

[32] I. Vlachos and G. Sergiadis, "Subsethood, entropy, and cardinality for interval-valued fuzzy sets – an algebraic derivation," *Fuzzy Sets Syst.*, vol. 158, pp. 1384–1396, 2007.

[33] D. Wu, "A constrained representation theorem for interval type-2 fuzzy sets using convex and normal embedded type-1 fuzzy sets, and its application to centroid computation," in *Proc. World Conf. Soft Comput.*, San Francisco, CA, USA, May 2011.

[34] D. Wu, "Approaches for reducing the computational cost of interval type-2 fuzzy logic systems: Overview and comparisons," *IEEE Trans. Fuzzy Syst.*, vol. 21, no. 1, pp. 80–99, Feb. 2013.

[35] D. Wu and J. Huang, "Ordered novel weighted averages," in *Type-2 Fuzzy Logic Syst.*, R. John, H. Hagras, and O. Castillo, Eds. New York, NY, USA: Springer, 2018, pp. 25–47.

[36] D. Wu and J. M. Mendel, "Aggregation using the linguistic weighted average and interval type-2 fuzzy sets," *IEEE Trans. Fuzzy Syst.*, vol. 15, no. 6, pp. 1145–1161, Dec. 2007.

[37] D. Wu and J. M. Mendel, "Cardinality, fuzziness, variance and skewness of interval type-2 fuzzy sets," in *Proc. 1st IEEE Symp. Found. Comput. Intell.*, Honolulu, HI, USA, Apr. 2007, pp. 375–382.

[38] D. Wu and J. M. Mendel, "Uncertainty measures for interval type-2 fuzzy sets," *Inf. Sci.*, vol. 177, no. 23, pp. 5378–5393, 2007.

[39] D. Wu and J. M. Mendel, "Corrections to 'aggregation using the linguistic weighted average and interval type-2 fuzzy sets,'" *IEEE Trans. Fuzzy Syst.*, vol. 16, no. 6, pp. 1664–1666, Dec. 2008.

[40] D. Wu and J. M. Mendel, "A vector similarity measure for linguistic approximation: Interval type-2 and type-1 fuzzy sets," *Inf. Sci.*, vol. 178, no. 2, pp. 381–402, 2008.

[41] D. Wu and J. M. Mendel, "A comparative study of ranking methods, similarity measures and uncertainty measures for interval type-2 fuzzy sets," *Inf. Sci.*, vol. 179, no. 8, pp. 1169–1192, 2009.

[42] D. Wu and J. M. Mendel, "Perceptual reasoning for perceptual computing: A similarity-based approach," *IEEE Trans. Fuzzy Syst.*, vol. 17, no. 6, pp. 1397–1411, Dec. 2009.

[43] D. Wu and J. M. Mendel, "Efficient algorithms for computing a class of subsethood and similarity measures for interval type-2 fuzzy sets," in *Proc. IEEE World Congr. Comput. Intell.*, Barcelona, Spain, 2010.

[44] D. Wu and J. M. Mendel, "Ordered fuzzy weighted averages and ordered linguistic weighted averages," in *Proc. IEEE World Congr. Comput. Intell.*, Barcelona, Spain, 2010.

[45] D. Wu, J. M. Mendel, and S. Coupland, "Enhanced interval approach for encoding words into interval type-2 fuzzy sets and its convergence analysis," *IEEE Trans. Fuzzy Syst.*, vol. 20, no. 3, pp. 499–513, Jun. 2012.

[46] D. Wu and W. W. Tan, "A simplified type-2 fuzzy controller for real-time control," *ISA Trans.*, vol. 15, no. 4, pp. 503–516, 2006.

[47] R. Yager, "A measurement-informational discussion of fuzzy union and fuzzy intersection," *Int. J. Man-Mach. Studies*, vol. 11, pp. 189–200, 1979.

[48] L. A. Zadeh, "The concept of a linguistic variable and its application to approximate reasoning-1," *Inf. Sci.*, vol. 8, pp. 199–249, 1975.

[49] L. A. Zadeh, "Fuzzy sets and information granularity," in *Proc. Adv. Fuzzy Set Theory Appl.*, M. Gupta, R. Ragade, and R. Yager, Eds. Amsterdam, the Netherlands: North-Holland Publishing Co., 1979, pp. 3–18.

[50] L. A. Zadeh, "Toward a theory of fuzzy information granulation and its centrality in human reasoning and fuzzy logic," *Fuzzy Sets Syst.*, vol. 19, pp. 111–127, 1997.

[51] L. A. Zadeh, "Toward a generalized theory of uncertainty (GTU)—An outline," *Inf. Sci.*, vol. 172, pp. 1–40, 2005.

[52] W. Zeng and H. Li, "Relationship between similarity measure and entropy of interval valued fuzzy sets," *Fuzzy Sets Syst.*, vol. 157, pp. 1477–1484, 2006.

[53] D. Zhai and J. M. Mendel, "Uncertainty measures for general type-2 fuzzy sets," *Inf. Sci.*, vol. 181, pp. 503–518, 2011.

Dongrui Wu (S'05–M'09–SM'14) received the B.E. degree in automatic control from the University of Science and Technology of China, Anhui Sheng, China, in 2003, an M.E. degree in electrical engineering from the National University of Singapore, Singapore, in 2005, and the Ph.D. degree in electrical engineering from the University of Southern California, CA, USA, in 2009.

He is now a Full Professor with the School of Automation, Huazhong University of Science and Technology, Wuhan, China. His research interests include affective computing, brain-computer interface, computational intelligence, and machine learning. He has authored more than 100 publications, including a book entitled *Perceptual Computing* (Wiley-IEEE, 2010).

Dr. Wu was the recipient of the IEEE CIS Outstanding Ph.D. Dissertation Award in 2012, the IEEE TRANSACTIONS on FUZZY SYSTEMS Outstanding Paper Award in 2014, the NAFIPS Early Career Award in 2014, and the IEEE SMC Society Early Career Award in 2017. He is an Associate Editor for the IEEE TRANSACTIONS ON FUZZY SYSTEMS, the IEEE TRANSACTIONS ON HUMAN-MACHINE SYSTEMS, and the IEEE COMPUTATIONAL INTELLIGENCE MAGAZINE.

Hai-Tao Zhang (M'07–S M'13) received the B.E. and Ph.D. degrees in automatic control from the University of Science and Technology of China, Hefei, China, in 2000 and 2005, respectively.

During January–December 2007, he was a Postdoctoral Researcher with the University of Cambridge, Cambridge, U.K. Since 2005, he has been with the Huazhong University of Science and Technology, Wuhan, China, where he was an Associate Professor from 2005 to 2010 and has been a Full Professor since 2010. His research interests include model predictive control, multiaxis machining, nanomanufacturing control and multiagent systems control.

Dr. Zhang serves as an Associate Editor for IEEE TRANSACTIONS ON CIRCUITS AND SYSTEMS II, *Scientific Reports*, and *Asian Journal of Control*, a Conference Editorial Board member for the IEEE Control Systems Society and the Chair of the IEEE CSS Wuhan Chapter.

Jian Huang (M'07–S M'17) received the B.E., M.Eng., and Ph.D. degrees in automatic control from the Huazhong University of Science and Technology (HUST), Wuhan, China, in 1997, 2000, and 2005, respectively.

From 2006 to 2008, he was a Postdoctoral Researcher with the Department of Micro-Nano System Engineering and the Department of Mechano-Informatics and Systems, Nagoya University, Japan. He is currently a Full Professor with the School of Automation, HUST. His research interests include rehabilitation robot, robotic assembly, networked control systems, and bioinformatics.